JEM Journal of Experimental Medicine

ARTICLE

# CXCL12+ dermal fibroblasts promote neutrophil recruitment and host defense by recognition of IL-17

Kellen J. Cavagnero[1], Fengwu Li[1], Tatsuya Dokoshi[1], Teruaki Nakatsuji[1], Alan M. O'Neill[1], Carlos Aguilera[1], Edward Liu[1], Michael Shia[1], Olive Osuoji[1], Tissa Hata[1], and Richard L. Gallo[1]

**The skin provides an essential barrier for host defense through rapid action of multiple resident and recruited cell types, but the complex communication network governing these processes is incompletely understood. To define these cell–cell interactions more clearly, we performed an unbiased network analysis of mouse skin during invasive *S. aureus* infection and revealed a dominant role for CXCL12+ fibroblast subsets in neutrophil communication. These subsets predominantly reside in the reticular dermis, express adipocyte lineage markers, detect IL-17 and TNFα, and promote robust neutrophil recruitment through NFKBIZ-dependent release of CXCR2 ligands and CXCL12. Targeted deletion of *Il17ra* in mouse fibroblasts resulted in greatly reduced neutrophil recruitment and increased infection by *S. aureus*. Analogous human CXCL12+ fibroblast subsets abundantly express neutrophil chemotactic factors in psoriatic skin that are subsequently decreased upon therapeutic targeting of IL-17. These findings show that CXCL12+ dermal immune acting fibroblast subsets play a critical role in cutaneous neutrophil recruitment and host defense.**

## Introduction

Acute injury or infection of barrier tissues such as the skin is typically characterized by the rapid recruitment of neutrophils and type 17 inflammatory response. Neutrophil recruitment is essential for host defense against *Staphylococcus aureus* (Mölne et al., 2000), a fact that is underscored by decades of observation of neutropenic patients at heightened risk of infection and severe disease (González-Barca et al., 2001; Bouma et al., 2010). Current models suggest that innate immune detection of *S. aureus* through pattern recognition receptors such as TLRs drives the expression of growth factors and chemokines including G-CSF, chemokine (C-X-C motif) ligand 1 (CXCL1), CXCL5, and CXCL8 (IL-8) that recruit neutrophils to the skin from the blood and bone marrow (Fournier and Philpott, 2005; Metzemaekers et al., 2020). Upon arrival, neutrophils directly kill *S. aureus* through several mechanisms including phagocytosis and the release of reactive oxygen species, antimicrobial peptides, and extracellular traps (Lehman and Segal, 2020).

Tissue-resident cells including epithelial keratinocytes and dendritic, lymphoid, and myeloid cell types also participate in defense against *S. aureus*. Keratinocytes have been the primary focus of most studies as these cells compose the outer layer of the epidermis and are a critical physical barrier. Keratinocytes detect *S. aureus* through the expression of functional pattern recognition and cytokine receptors. Following detection of *S. aureus*, the epidermis produces neutrophil chemokines and multiple antimicrobial peptides (Schauber and Gallo, 2009), and conditional knockout mice have demonstrated a significant role for keratinocytes in neutrophil recruitment and host defense (Moos et al., 2019, 2023). Decades of *in vitro* observations have hinted that fibroblasts)—cells appreciated largely for their role in supporting tissue architecture and scar formation—may also contribute to innate immune defense (Davidson et al., 2021; Cavagnero and Gallo, 2022). Indeed, in 2015, a preadipocyte subset of dermal fibroblasts was shown to be triggered by invasive *S. aureus* infection to develop into adipocytes and express the antimicrobial peptide cathelicidin (also known in humans as LL-37 and encoded by *CAMP*) (Zhang et al., 2015), a potent antimicrobial and immune regulating peptide required for defense against invasive infections (Nizet et al., 2001). Nevertheless, a significant role in skin neutrophilia and host defense for dermal fibroblasts—as a whole or any subset—has not been demonstrated.

To understand the cell–cell interactions underlying skin inflammation and host defense more clearly, we leveraged single-cell RNA sequencing (scRNA-Seq) and unbiased network analysis of skin during *S. aureus* infection in mice and other models of skin neutrophilic inflammation in mice and humans. Our work revealed that CXCL12+ dermal fibroblast subsets are

[1]Department of Dermatology, University of California, San Diego. La Jolla, CA, USA.

Correspondence to Richard L. Gallo: rgallo@health.ucsd.edu.

major mediators of neutrophil recruitment to the skin and play an important role in host defense through their recognition of IL-17 and TNF. These findings uncover a critical and previously unappreciated role for dermal fibroblasts to coordinate cutaneous inflammation and host defense.

## Results

### CXCL12+ subsets of dermal fibroblasts communicate with neutrophils during infection by *S. aureus*

To better understand the host defense response of the skin against *S. aureus* infection, we performed droplet-based scRNA-Seq and unbiased network analysis of mouse back skin 1 day after intradermal (i.d.) infection with methicillin-resistant *S. aureus* (MRSA) (Fig. 1 A). Major cell lineages recovered were clustered and identified based on marker genes as fibroblasts, keratinocytes, myeloid cells, lymphoid cells, endothelial cells, mural cells, melanocytes, Schwann cells, and skeletal muscle cells (Fig. 1 B and Fig. S1 A). As expected, myeloid cells, a lineage that includes neutrophils, increased in frequency following infection (Fig. 1 C). Network analysis using CellChat (Jin et al., 2021) revealed that the dominant communication input myeloid cells received was sent from fibroblasts (Fig. 1 D). This observation differed from current models of early skin defense against *S. aureus* that have focused the greatest attention on signals between epithelial keratinocytes and myeloid cells (Miller and Cho, 2011; Moos et al., 2023).

To identify mediators used by dermal fibroblasts to communicate with myeloid cells, we next performed differential expression analysis on fibroblasts and identified upregulated genes during infection including neutrophil chemokines (*Cxcl1*, *Cxcl2*, *Cxcl3*, *Cxcl5*, and *Cxcl12*), neutrophil growth factors (*Csf3*), pro-neutrophilic cytokines (*Il33* and *Il6*), and other host defense genes with potential roles in neutrophil recruitment (*Lcn2*, *Mif*, and *C3*) (Fig. 1 E) (Capucetti et al., 2020; Shao et al., 2016; Stark et al., 2013; Zheng et al., 2021; Enoksson et al., 2013; Rose-John et al., 2017; Mehta and Corey, 2021). Gene set enrichment analysis (GSEA) of the differentially expressed genes (DEGs) in dermal fibroblasts showed that IL-17 signaling was a highly upregulated pathway during infection (Fig. 1 F). Fibroblast expression of IL-17 signaling and *Cxcl1*, *Cxcl5*, *Cxcl12*, *Lcn2*, and *Il17ra* was greater than other cell types (Fig. 1 G).

Time-course analysis of neutrophil chemokines by quantitative PCR (qPCR) and GR-1 by immunofluorescence (marks predominantly neutrophils; Hestdal et al., 1991; Boehme et al., 2009) demonstrated that *Cxcl1*, *Cxcl5*, and neutrophils increased in the skin as early as 3 h after infection, and *Cxcl12*, which had high baseline expression, increased within 24 h (Fig. 1 H and Fig. S1 B). Neutrophil levels peaked shortly after *Cxcl1* and *Cxcl5* and shortly before *Cxcl12*. After 2 days, *Cxcl1*, *Cxcl5*, *Cxcl12*, and neutrophil levels declined and reached baseline levels by day 10. These results suggest that fibroblast *Cxcl1* and *Cxcl5* may be important for early neutrophil recruitment and fibroblast *Cxcl12* for late neutrophil recruitment and retention.

Dermal fibroblasts are becoming appreciated as heterogeneous and multifunctional (Cavagnero and Gallo, 2022). To understand which fibroblast subsets communicate with neutrophils, we next interrogated the fibroblast subpopulations in our dataset using unsupervised clustering. This analysis identified 11 clusters of fibroblasts (FBs) with distinct expression of marker genes (Fig. 1 I and Fig. S1 C). Clusters FB1, FB3–FB6, and FB10 increased in frequency during infection, while FB2, FB7–FB9, and FB11 decreased (Fig. S1 D). Plotting expression of known markers for papillary, reticular, adipocyte lineage, and myofibroblast subsets (Table S1) identified FB1–FB7 as reticular and adipocyte lineage clusters and FB8–FB11 as papillary and myofibroblast clusters (Fig. 1 J). Unbiased differential expression, pathway, and network analyses confirmed this finding and revealed functions of reticular and adipocyte lineage cells in recognition of IL-17 and host defense (i.e., "positive regulation of defense response" and "neutrophil migration") and papillary and myofibroblasts in matrix production ("skin development") (Fig. 1, K and L; and Fig. S1 E). Indeed, expression of neutrophil chemokines *Cxcl1*, *Cxcl2*, *Cxcl3*, *Cxcl5*, and *Cxcl12* was enriched in FB1–FB7 (Fig. 1 M). Notably, clusters within FB1–FB7 expressed unique profiles of neutrophil chemokines. For example, *Cxcl12* was broadly expressed by FB1–FB7, whereas *Cxcl5* was observed primarily in FB1. To characterize neutrophil recruiting fibroblast subsets more precisely, we classified dermal fibroblasts during *S. aureus* infection as neutrophil chemokine+ (defined as expressing *Cxcl1*, *Cxcl2*, *Cxcl3*, *Cxcl5*, or *Cxcl12*) or neutrophil chemokine− (defined as lacking *Cxcl1*, *Cxcl2*, *Cxcl3*, *Cxcl5*, and *Cxcl12* expression) and found that 84% of neutrophil chemokine+ cells belonged to reticular and adipocyte lineage clusters FB1–FB7 and 16% belonged to papillary and myofibroblasts clusters FB8–FB11 (Fig. S1, F and G). Differential expression analysis comparing neutrophil chemokine+ and neutrophil chemokine− fibroblasts indicated that *Cxcl12* was a highly sensitive and specific marker of neutrophil chemokine+ fibroblasts (Fig. 1, N and O). Confocal microscopy confirmed that CXCL1 and CXCL12 were expressed by fibroblasts in the dermis after *S. aureus* infection, with more staining of fibroblasts in the deeper reticular dermis and in the perifollicular regions than fibroblasts located in the upper papillary dermis (Fig. 1 P).

To determine whether deep dermal fibroblast involvement was driven by i.d. challenge, we analyzed scRNA-Seq data from mice following epicutaneous *S. aureus* infection (Nakatsuji et al., 2023). This analysis revealed that, of all skin cell lineages, subsets of dermal fibroblasts expressed the highest levels of neutrophil chemokines (Fig. S1 H), with 75% of neutrophil chemokine+ fibroblasts belonging to clusters marked by reticular and adipocyte lineage genes (Fig. S1, I–N). Neutrophil chemokine+ fibroblasts during topical infection shared many markers with neutrophil chemokine+ fibroblasts during i.d. infection, including *Cxcl12* (Fig. S1, O and P).

Taken together, these results suggest that CXCL12+ fibroblast subsets, largely found in the lower dermis, are poised to produce chemokines, growth factors, and cytokines to recruit and activate neutrophils in response to *S. aureus* infection and that this response could be triggered by IL-17.

### Host defense response by CXCL12+ adipocyte lineage fibroblasts is activated by IL-17 and TNF

Having identified adipocyte lineage genes enriched in CXCL12+ dermal fibroblast subsets, we next directly tested function

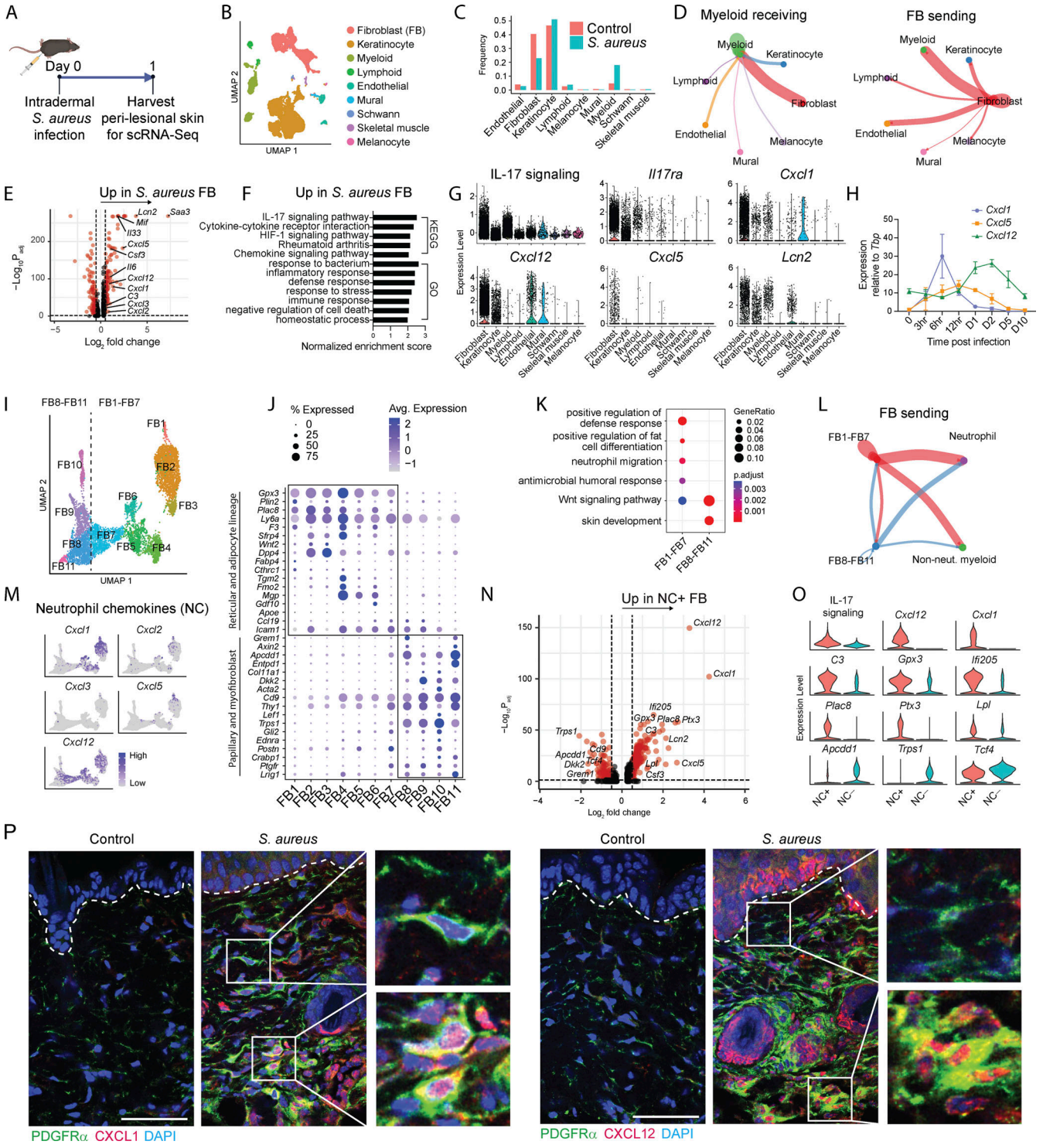


Figure 1. **Skin response to *S. aureus* infection reveals IL-17–mediated CXCL12+ dermal fibroblast–neutrophil communication. (A)** *S. aureus* (USA300 LAC strain) i.d. infection model. **(A–G and I–O)** scRNA-Seq of back skin. Data were obtained from samples pooled from $N = 4$ mice independently treated in each group. **(B)** Dimensionality reduction colored by cell type in control (vehicle) and infected mice. **(C)** Proportion of each cell type in control and infected mice. **(D)** Network analysis showing communication toward myeloid cells (left) and from fibroblast (right). Edge weight is proportional to communication strength. Edge and node color indicates communication source. **(E)** DEGs in fibroblast during infection using Wilcoxon Rank Sum test. $Log_2$ fold-change and P value (adjusted) cut-offs are 0.5 and 0.05, respectively. **(F)** GSEA of fibroblasts using Kyoto encyclopedia of genes and genomes (KEGG) and gene ontology (GO) databases. **(G)** Expression of IL-17 signaling score and specific genes related to IL-17 signaling across cell types. **(H)** Gene expression by qPCR over time following *S. aureus* infection using bulk skin samples. Data are means ± SEM and representative of two independent experiments with $N = 3$ mice. **(I)** Fibroblast dimensionality reduction colored by cluster. The dashed line separates FB1–FB7 and FB8–FB11. **(J)** Expression of fibroblast subset markers across clusters. Boxes highlight high expression of reticular and adipocyte lineage genes in FB1–FB7 and high expression of papillary and myofibroblast genes in FB8–FB11. **(K)** GO term analysis comparing FB1–FB7 and FB8–FB11. **(L)** Network analysis showing outgoing communication from FB1–FB7 and FB8–FB11 toward

neutrophils and other myeloid cells. Edge weight is proportional to communication strength. Edge and node color indicates communication source. **(M)** Neutrophil chemokine expression across fibroblast clusters. **(N)** DEGs between neutrophil chemokine+/− fibroblasts during infection using Wilcoxon Rank Sum test. $Log_2$ fold-change and P value (adjusted) cut-offs are 0.5 and 0.05, respectively. **(O)** Expression of neutrophil chemokine+/− fibroblast markers during infection. **(P)** Representative confocal CXCL1 and CXCL12 immunostaining in skin 2 days after *S. aureus* infection and control. Upper inset, papillary. Lower inset, reticular. Scale bar, 50 µm. Dashed line represents epidermal–dermal junction.

*in vitro* with the murine preadipocyte fibroblast cell line 3T3-L1. These cells were chosen because they can be induced *in vitro* to undergo fat-cell differentiation and express adipocyte lineage markers like the dermal fibroblast subsets observed *in vivo* (Fig. 1, J and K). To first test if IL-17–producing cells could activate preadipocyte fibroblasts, conditioned media (CM) from T helper 17 (Th17) cells generated in culture was added to 3T3-L1s (Fig. 2 A). Th17 CM induced expression of neutrophil chemokine *Cxcl1* and antimicrobial *Lcn2* in 3T3-L1s and a role for IL-17 from these T cells was confirmed by the addition of neutralizing antibodies against IL-17A (Fig. 2 B). Stimulation of 3T3-L1s with recombinant IL-17A was also sufficient to induce low levels of neutrophil chemokine and antimicrobial expression (Fig. 2 C). These observations in 3T3-L1 cells were consistent with prior reports using mixed primary dermal fibroblasts (Fossiez et al., 1996; Ha et al., 2014) and supported our findings that adipocyte lineage subsets within the heterogenous dermal fibroblast populations can respond to IL-17 by production of chemotactic and antimicrobial factors.

In addition to the expression of IL-17 in the skin, invasion by *S. aureus* promotes the expression of several other inflammatory host defense genes and exposes dermal fibroblasts to bacterial products including TLR ligands. Therefore, we next screened several purified TLR ligands and recombinant proinflammatory cytokines to identify additional potential triggers of CXCL12+ fibroblast subsets. This screen revealed that TNFα, IL-1β, and ligands for TLR1/2, TLR2/6, and TLR4 induced 3T3-L1 to express neutrophil chemokines and antimicrobials (Fig. 2 C and Fig. S2 A). Since IL-17A can potentiate the effect of several innate immune stimuli (McGeachy et al., 2019; Li et al., 2019), we next tested the response to IL-1β, TNFα, and MALP-2 (a TLR2/6 ligand) in the presence and absence of IL-17A. IL-17A robustly synergized with TNFα to drive 3T3-L1 expression of *Cxcl1* and *Lcn2* (Fig. 2 C). IL-17F, which binds to the same receptor as IL-17A, also potentiated TNF-induced activation but was less potent than IL-17A (Fig. S2 B). siRNA knockdown of *Tnfrsf1a* indicated that the preadipocyte *Lcn2* response to TNFα was TNFR1 dependent (Fig. S2 C). The synergistic effect of IL-17A and TNFα was also observed in primary mouse dermal fibroblasts (MDFBs) (Fig. S2 D), and the use of MDFBs isolated from *Tnfrsf1a*$^{-/-}$ mice eliminated synergy but did not eliminate the *Lcn2* response to IL-17A (Fig. S2 E). We also tested whether other cytokines produced by Th17 cells were sufficient to induce *Lcn2* expression. IL-22 had no effect alone and did not synergize with IL-17A; IFNγ had no effect alone and synergized with IL-17A but to a lesser extent than TNFα (Fig. S2 D).

We next performed an unbiased investigation into the effect of IL-17A and TNFα on 3T3-L1 using bulk RNA-Seq. The effect of these proinflammatory cytokines was compared with the response when these preadipocyte fibroblasts were stimulated to undergo adipogenesis, which we previously showed induced the expression of *Camp*, an antimicrobial peptide and inflammatory mediator (Zhang et al., 2015). IL-17A and TNFα induced broad transcriptional changes that were different than those induced during adipogenesis (Fig. 2 D). IL-17A alone did not induce major differences in gene expression compared with TNFα (36 versus 885 DEGs), though it potentiated TNF-induced gene expression and drove expression of genes induced by neither cytokine alone (Fig. 2 D). Genes upregulated by IL-17A and TNFα were consistent with NF-κB signaling, neutrophil migration, and host defense including *Nfkbiz*, *Cxcl1*, *Cxcl5*, *Cxcl12*, *Camp*, *Lcn2*, *C3*, *Mif*, and *Csf3* (Fig. 2, E and F). Similar results were observed in MDFBs and human subcutaneous preadipocyte (HPAD) fibroblasts after the addition of IL-17A and TNFα (Fig. 2 G and Fig. S2, F–I).

To further understand the effect of IL-17A and TNFα on CXCL12+ dermal fibroblasts, we probed 3T3-L1 preadipocyte fibroblast CM using a multiplex immunoassay. Secretion of 12 out of 13 chemokines assayed, including neutrophil chemokines CXCL1 and CXCL5, was synergistically induced by IL-17A and TNFα (Fig. 2 H). Importantly, CXCL12 was highly expressed at baseline—confirming the identity of this cell line as CXCL12+ adipocyte lineage—and induced by IL-17A and TNFα (Fig. 2 I). Western blot of 3T3-L1 CM showed that lipocalin 2 (LCN2) secretion was elicited potently by combined treatment with IL-17A and TNFα and moderately by adipogenesis (Fig. 2 J). Protein expression of CXCL1, CXCL12, CRAMP, and LCN2 was also observed by flow cytometry and immunostaining of 3T3-L1s and MDFBs (Fig. 2, K–M; and Fig. S2, J–K), and protein secretion of CXCL8 was observed by ELISA of HPAD CM (Fig. S2 L). Interestingly, IL-17 increased both CXCL1 secretion (Fig. 2 H) and intracellular CXCL1 expression when secretion was inhibited (Fig. 2 K) but decreased intracellular CXCL1 expression when secretion was not inhibited (Fig. 2 L), suggesting that IL-17 may activate machinery for secretion of translated neutrophil chemokines.

We next investigated the signaling pathways activated in CXCL12+ adipocyte lineage fibroblasts by IL-17A and TNFα. Most studies investigating the mechanisms underlying synergistic activation by IL-17A and TNFα have utilized epithelial cells and osteoblasts (Karlsen et al., 2010). These prior studies demonstrated that TNFα-induced NF-κB signaling drives transcription of primary response genes including proinflammatory cytokines and the NF-κB cofactor NFKBIZ, and that IL-17A signaling activates RNA binding proteins to promote the stabilization of the TNFα-induced transcripts (Li et al., 2019). Stabilization of NFKBIZ mRNA facilitates its translation and binding to nuclear NF-κB for further transcriptional regulation of secondary response genes, that is gene- and cell-type specific (Karlsen et al., 2010). We found that in 3T3-L1 preadipocytes, TNFα alone

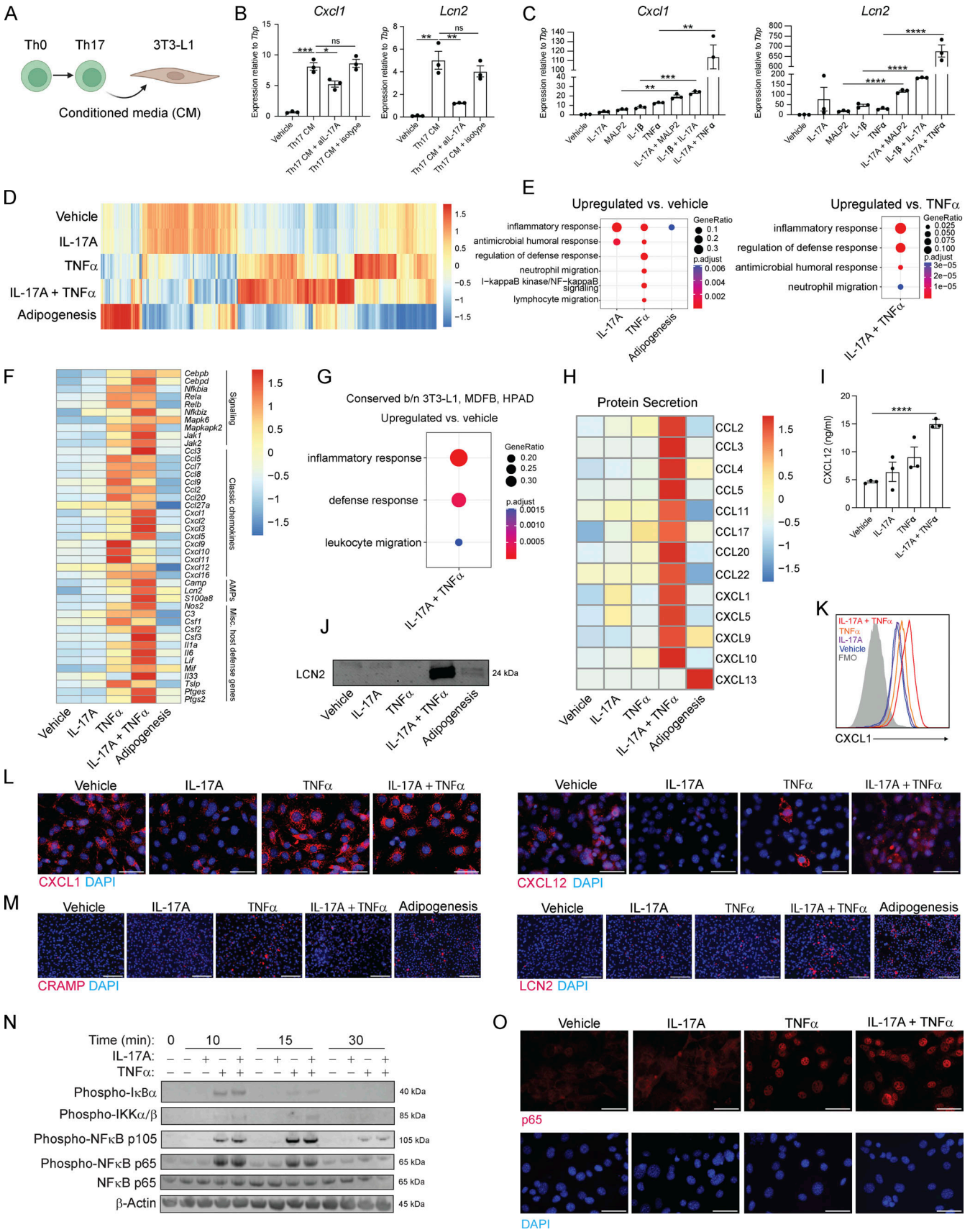


Figure 2. **IL-17 synergizes with TNFα to induce preadipocyte fibroblast NF-κB and production of neutrophil chemokines. (A)** Schematic of in vitro assay to test the effect of Th17 CM on fibroblasts used in B. **(B)** 3T3-L1 fibroblast gene expression by qPCR following treatment with Th17 CM ± anti–IL-17A

blocking antibody (aIL-17A) or control isotype antibody. **(C)** Recombinant cytokine-stimulated 3T3-L1 gene expression by qPCR. **(D–G)** Bulk RNA-Seq of 3T3-L1 cells. Data were obtained from samples pooled from $N = 3$ independent biological replicates in each group. **(D)** Expression of top 2,000 genes with the highest variance between groups, scaled by column. **(E)** GO analysis of genes upregulated compared to vehicle control (left) and TNFα (right). **(F)** Expression of select genes, scaled by row. **(G)** GO analysis of upregulated genes conserved among TNFα and IL-17A treated 3T3-L1s, primary MDFBs, and HPADs. **(H)** Multiplex immunoassay of 3T3-L1 CM, scaled by row. Averages shown for $N = 3$. **(I)** CXCL12 ELISA of 3T3-L1 CM. **(J)** Representative LCN2 western blot of 3T3-L1 CM. **(K)** Representative CXCL1 intracellular cytokine staining in 3T3-L1s. **(L)** Representative CXCL1 and CXCL12 immunostaining in 3T3-L1s. Scale bar, 50 µm. **(M)** Representative CRAMP and LCN2 immunostaining in 3T3-L1s. Scale bar, 150 µm. **(N)** Representative phosphorylation (phospho) western blots in 3T3-L1s. **(O)** Representative p65 immunostaining in 3T3-L1s. Scale bar, 50 µm. Data in B–O are representative of at least two independent experiments with $N = 3$. Error bars represent SEM. FMO, fluorescence minus one; AMPs, antimicrobial peptides; ns (not significant), *P < 0.05, **P < 0.01, ***P < 0.001, and ****P < 0.0001 using unpaired *t* test. Source data are available for this figure: SourceData F2.

induced transient phosphorylation of canonical NF-κB signaling molecules IKKα/β, p105, and p65 within 10 min of activation (Fig. 2 N). No effect was detected on NF-κB signaling by IL-17A alone. Evaluation of nuclear translocation of p65 showed a similar response (Fig. 2 O), demonstrating that IL-17A did not mediate the synergistic upregulation of neutrophil chemokines in 3T3-L1 by enhancing NF-κB signaling and that IL-17A may work in these preadipocyte fibroblasts by activating RNA binding proteins to stabilize NFKBIZ. Indeed, the NF-κB cofactor *Nfkbiz* was highly expressed in the dermal adipocyte lineage fibroblasts during *S. aureus* infection of the skin (Fig. S1 E), and in vitro stimulation with IL-17A and TNFα synergistically induced NFKBIZ gene expression in 3T3-L1s, MDFBs, and HPADs (Fig. 2 F and Fig. S2, M and N). Inhibition experiments with genetic approaches defined the dependence on NFKBIZ for preadipocytes to respond to IL-17A and TNFα: bulk RNA-Seq of 3T3-L1s following *Nfkbiz* siRNA knockdown revealed that NFKBIZ was required for IL-17A– and TNFα-induced expression neutrophil chemokines and antimicrobials and that NFKBIZ suppressed the expression of myeloid cell and lymphocyte chemoattractants (Fig. 3 A and Fig. S3, A and B). These results were validated by qPCR (Fig. S3 C). Unlike inhibition of NFKBIZ, inhibition of other pathways activated by IL-17A and TNFα including JNK, P38 MAPK, JAK, or HIF1A did not lead to a broad reduction of neutrophil chemokine gene expression (Fig. S3, D–G).

Collectively, these findings demonstrate that IL-17 synergizes with several innate immune stimuli—especially TNFα—to activate mouse and human preadipocyte fibroblast NFKBIZ and increase the secretion of an array of neutrophil chemokines including CXCL12. This further supports our earlier *in vivo* observations that CXCL12+ subsets of dermal fibroblasts, primarily found in the deep dermis with high expression of genes consistent with IL-17 signaling and adipocyte lineage cells, communicate with neutrophils during *S. aureus* skin infection.

### CXCL12+ adipocyte lineage fibroblasts activate and induce migration of neutrophils

We next sought to directly evaluate the functional impact of CXCL12+ fibroblast communication with neutrophils. Purified bone marrow neutrophils (>98%) were stimulated with CM from 3T3-L1 preadipocytes following siRNA knockdown of *Nfkbiz* or control and subsequent activation by IL-17A and TNFα (Fig. 3 B and Fig. S4 A). Bulk RNA-Seq identified 478 genes that were upregulated in neutrophils by preadipocytes activated with IL-17A and TNFα (Fig. 3, C and D). Pathway analysis using the genes upregulated in neutrophils both in vitro and in vivo during *S. aureus* infection suggested that CXCL12+ fibroblasts treated with IL-17A and TNFα secrete factors that prime neutrophils for host defense (i.e., "positive regulation of cell migration," "inflammatory response," and "regulation of defense response") (Fig. 3 E). Upregulated genes included the proinflammatory cytokine *Il1b* as well as *Il1r2* and *Il1rn*, which have been shown to be conserved neutrophil activation markers (Grieshaber-Bouyer et al., 2021) (Fig. 3 F). Remarkably, the expression of most genes upregulated by neutrophils *in vitro* and *in vivo* was dependent on fibroblast NFKBIZ (Fig. 3 F). Expression of *Il1b*, *Il1r2*, and *Il1rn* was validated by qPCR (Fig. S4 B).

A transwell migration assay was applied next to evaluate the capacity of CXCL12+ dermal fibroblasts to promote neutrophil migration (Fig. 3 G). Whereas CM from 3T3-L1s activated by IL-17A or TNFα alone induced moderate leukocyte migration, CM from 3T3-L1s stimulated with IL-17A and TNFα together promoted robust leukocyte migration (Fig. 3 H). To confirm that IL-17A and TNFα present in the CM did not induce neutrophil migration, recombinant IL-17A and TNFα were also tested as a control without preadipocytes and observed to have no direct effect on migration (Fig. 3 H). Flow cytometric analysis of the migrated cells revealed that neutrophil migration was induced sixfold, monocyte migration threefold, and lymphocyte migration twofold (Fig. 3 I and Fig. S4 C). Similar findings were observed with MDFBs (Fig. S5 D). MDFBs derived from *Tnfrsf1a*$^{-/-}$ mice elicited significantly less neutrophil migration when stimulated with IL-17A and TNFα, validating the requirement of TNFR1 for fibroblast–neutrophil communication in response to TNFα (Fig. 3 J). CM from 3T3-L1s stimulated with IL-17A and TNFα also promoted robust migration when using purified neutrophils (Fig. S4 E). In contrast to the response to IL-17A and TNFα, preadipocytes did not induce neutrophil migration when activated by differentiation into adipocytes, suggesting that *Camp* and *Lcn2* may not mediate migration (Fig. S4 F).

We next investigated which mediators produced by CXCL12+ dermal fibroblasts drive neutrophil migration. Administration of pertussis toxin to inhibit G protein–coupled receptors (Metzemaekers et al., 2020) severely suppressed neutrophil migration (Fig. 3 K). *Nfkbiz* knockdown, which we observed to inhibit preadipocyte expression of neutrophil chemokines, also resulted in significantly less neutrophil recruitment (Fig. 3 L). Experiments using MDFB derived from *Lcn2*$^{-/-}$ and *Camp*$^{-/-}$ (encoding the peptide CRAMP) mice, and experiments using a pharmacologic macrophage migration inhibitory factor (MIF) inhibitor indicated that these host defense genes with

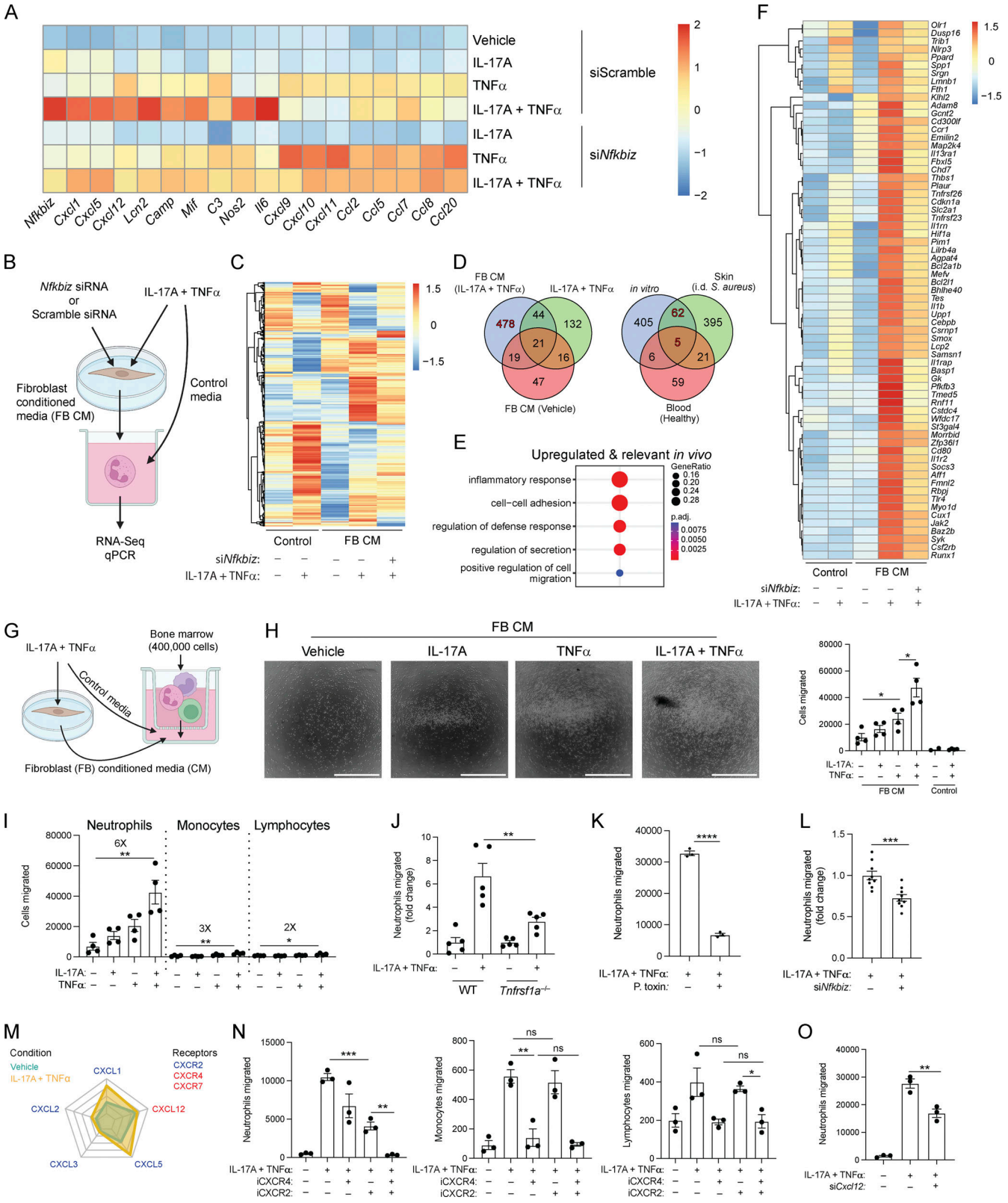


Figure 3. **Preadipocyte fibroblasts activate and recruit neutrophils using the master transcriptional regulator NFKBIZ. (A)** 3T3-L1 fibroblast gene expression by bulk RNA-Seq following *Nfkbiz* or control siRNA knockdown, scaled by column. Data were obtained from samples pooled from *N* = 3 independent biological replicates in each group. **(B)** Schematic for 3T3-L1 CM induced neutrophil activation assay used in C–F. Bulk RNA-Seq data were obtained from samples pooled from *N* = 3 independent biological replicates in each group. **(C)** Expression of top 2,000 variable genes, scaled by row. **(D)** Identification of genes specifically upregulated in neutrophils by activated fibroblasts (left, 478 genes, highlighted in red) and identification of the in vivo relevant subset (right, 67 genes, highlighted in red). **(E)** GO analysis of the 67 in vivo relevant genes. **(F)** Expression of the 67 in vivo relevant genes in neutrophils following stimulation

with fibroblast CM, scaled by row. **(G)** Schematic for 3T3-L1 CM induced leukocyte migration assay used in H–P. **(H)** Representative images of migrated leukocytes (left) and quantification (right). Scale bar, 750 µm. **(I)** Migrated leukocyte subsets. Multiplier indicates fold increase. **(J)** Neutrophil migration assay using *Tnfrsf1a*$^{-/-}$ primary MDFB CM. Data were pooled from two independent experiments with $N = 2–3$. **(K)** Neutrophils migrated following pertussis toxin (P. toxin) treatment. **(L)** Neutrophils migrated using CM from 3T3-L1 following *Nfkbiz* siRNA knockdown. Data were pooled from three independent experiments with $N = 3$. **(M)** 3T3-L1 gene expression of neutrophil chemokines with corresponding receptors from bulk RNA-Seq in Fig. 2. Data were obtained from samples pooled from $N = 3$ independent biological replicates in each group. **(N)** Neutrophils, monocytes, and lymphocytes migrated following pharmacological inhibitor pretreatment. **(O)** Neutrophils migrated using CM from 3T3-L1 following *Cxcl12* or control siRNA knockdown. Data in A, C–I, K, and M–O are representative of at least two independent experiments with $N = 3$. Error bars represent SEM. ns (not significant), *P < 0.05, **P < 0.01, ***P < 0.001, and ****P < 0.0001 using unpaired *t* test.

purported neutrophil chemotactic function are not required for fibroblasts to promote neutrophil migration (Fig. S4, G–I). Radar plot of relative gene expression by 3T3-L1s showed that these cells express multiple CXCR2 ligands (CXCL1, CXCL2, CXCL3, and CXCL5) and CXCR4/7 ligand CXCL12 following activation by IL-17A and TNFα (Fig. 3 M) (Balabanian et al., 2005; Metzemaekers et al., 2020). Pharmacological inhibition of CXCR2 reduced neutrophil migration but not monocyte or lymphocyte migration (Fig. 3 N). Purified bone marrow neutrophils expressed higher levels of CXCR4 than CXCR7 (Fig. S4 J). Pharmacological inhibition of CXCR4 reduced neutrophil migration and abrogated monocyte and lymphocyte migration. Combined inhibition of CXCR2 and CXCR4 abrogated neutrophil migration. Similar results were observed in MDFBs (Fig. S4 K). Corroborating these findings, *Cxcl12* siRNA knockdown in fibroblasts partially reduced neutrophil, monocyte, and lymphocyte recruitment (Fig. 3 O and Fig. S4 L). Taken together, these results show that CXCL12+ fibroblasts activated with IL-17A and TNFα secrete NFKBIZ-dependent CXCR2 ligands and CXCL12 that drive neutrophil migration.

### Skin inflammation and host defense by fibroblast recognition of IL-17

To determine the importance of CXCL12+ dermal fibroblasts for neutrophil recruitment and inflammation, we developed mice lacking IL-17RA specifically in fibroblasts by crossing *Il17ra*$^{fl/fl}$ mice with *Pdgfra*$^{Cre}$ mice (*Pdgfra*$^{\Delta Il17ra}$), a Cre driver that targets fibroblasts with high fidelity (Chung et al., 2018; Boothby et al., 2021; Xu et al., 2021; Zhang et al., 2016). Because dermal fibroblasts express IL-17RA, IL-17RC, and IL-17RD but not IL-17RB nor IL-17RE (Fig. S5 A), this approach likely eliminates fibroblast response to IL-17A/F but not IL-17B, IL-17C, or IL-17E (IL-25). (Li et al., 2019). Validating the specificity of the conditional knockout, *Il17ra* expression in *Pdgfra*$^{\Delta Il17ra}$ mice was maintained in the epidermis, reduced in the dermis, and nearly eliminated from isolated dermal fibroblasts (Fig. 4 A and Fig. S5 B). Further, dermal fibroblasts isolated from *Pdgfra*$^{\Delta Il17ra}$ mice demonstrated a severely attenuated response to IL-17A and TNFα as assessed by *Cxcl1* expression (Fig. 4 B).

To model IL-17–dependent inflammation in vivo, recombinant IL-17A and TNFα were injected i.d. into the back skin of WT mice to induce neutrophil recruitment after 72 h (Fig. 4, C and D). *Pdgfra*$^{\Delta Il17ra}$ mice showed less skin erythema, reduced expression of neutrophil chemokines and other host defense genes, and far fewer neutrophils in the skin following administration of IL-17A and TNFα (Fig. 4, E–J). Monocytes and macrophages were slightly decreased in *Pdgfra*$^{\Delta Il17ra}$ mice (Fig. S5 C). We next challenged the back skin of *Pdgfra*$^{\Delta Il17ra}$ mice i.d. with *S. aureus* (Fig. 4 K). A USA300-lac (MRSA) strain equipped with an *agrI* quorum sensing reporter was used to enable the assessment of bacterial density and virulence factor production (Hall et al., 2013). Targeted deletion of IL-17RA in fibroblasts resulted in reduced expression of neutrophil chemokines and other host defense genes (Fig. 4 L), reduced neutrophil recruitment (Fig. 4 M), increased *S. aureus* reporter expression (Fig. 4 N), and larger lesions at 24 and 48 h after infection (Fig. 4 O). Similar levels of monocytes and macrophages were observed in control and transgenic mice infected with *S. aureus* (Fig. S5 D). Together, these results demonstrate that fibroblast IL-17 signaling is critical for skin neutrophil recruitment and host defense against *S. aureus*.

To determine the potential role of CXCL12+ dermal fibroblast subsets in other forms of type 17 inflammation, we next performed scRNA-Seq on back skin from mice treated topically with imiquimod (IMQ), a common model of type 17 inflammation (Gangwar et al., 2022) (Fig. 5 A). Cell types recovered were identified based on marker genes as fibroblasts, keratinocytes, myeloid cells, lymphoid cells, melanocytes, mural cells, and endothelial cells (Fig. S5 E). As expected, myeloid cells and keratinocytes increased in frequency following 5 days of IMQ (Fig. S5 F). As with the response to *S. aureus*, network analysis showed that myeloid cells received more input from fibroblasts following IMQ challenge compared with other cell types (Fig. 5 B). Compared with fibroblasts from control mice, fibroblasts from IMQ-treated mice upregulated genes consistent with IL-17 signaling and neutrophil recruitment including *Nfkbiz*, *Cxcl1*, *Cxcl2*, *Cxcl3*, and *Cxcl12* (Fig. 5, C and D). Compared with epidermal cells, dermal cells expressed greater levels of *Cxcl1* and *Cxcl12* (Fig. S5, G and H). Targeted deletion of IL-17RA in fibroblasts using *Pdgfra*$^{\Delta Il17ra}$ mice resulted in reduced expression of IMQ-induced neutrophil chemokines and other inflammatory genes (Fig. 5 E). Microscopy confirmed that IMQ-induced expression of CXCL1 and CXCL12 was dependent on fibroblast IL-17 signaling (Fig. 5 F). In line with these findings, *Pdgfra*$^{\Delta Il17ra}$ mice had significantly reduced IMQ-induced neutrophil recruitment to the skin, particularly in the perifollicular region (Fig. 5, G–I; and Fig. S5 I). No change was observed in the number of monocytes and macrophages (Fig. S5 J).

### IL-17 promotes communication between CXCL12+ dermal fibroblasts and neutrophils in psoriasis

Our observation that CXCL12+ dermal fibroblast subsets play an important role during infectious and non-infections forms of type 17 inflammation in mice led us to next ask if similar subsets

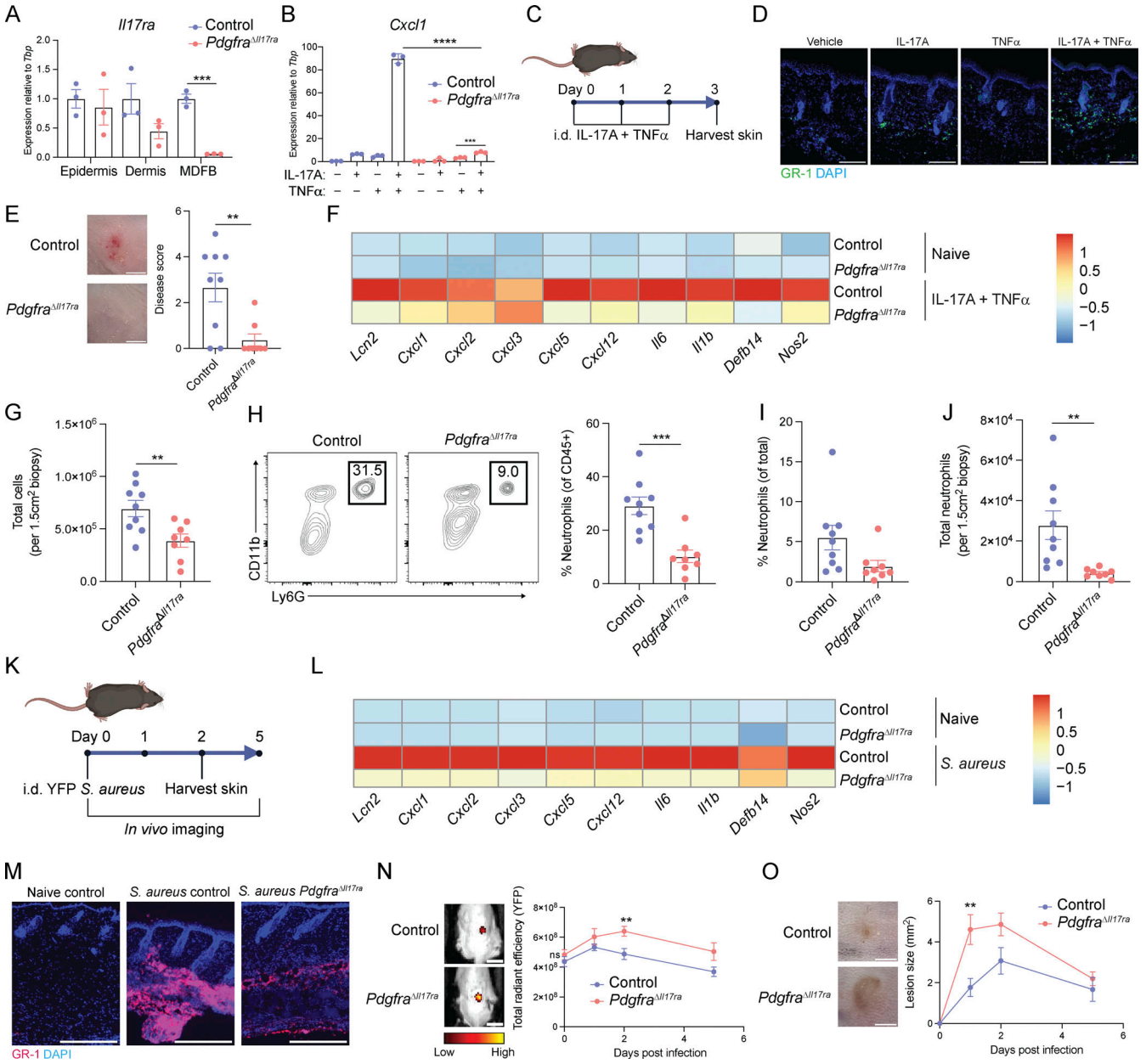


Figure 4. **Fibroblast IL-17 signaling is required for neutrophil recruitment to the skin and defense against *S. aureus*.** **(A)** *Il17ra* expression in separated epidermis, dermis, and isolated dermal fibroblasts (MDFB) from the skin of *Pdgfra*-Cre × *Il17ra* fl/fl (*Pdgfra*$^{\Delta Il17ra}$) conditional knockout mice and control Cre− littermates. Data are representative of two independent experiments with *N* = 3 mice. **(B)** MDFB gene expression by qPCR following in vitro stimulation. Data are representative of two independent experiments with *N* = 3. **(C)** Schematic of recombinant cytokine-induced model of *in vivo* neutrophil recruitment used in D–J. **(D)** Representative GR-1 (neutrophil) immunostaining in WT mice. Scale bar, 150 µm. **(E–J)** Recombinant cytokine injection model with *Pdgfra*$^{\Delta Il17ra}$ and Cre− littermates (control). The experiment was performed three times with *N* = 2–3 mice per independent experiment. Naïve skin was harvested in a separate experiment with *N* = 3 mice. **(E)** Representative images of mouse skin and quantification of inflammation. Scale bar, 3 mm. **(F)** Expression of neutrophil chemokines, proinflammatory cytokines, and other host defense genes by qPCR, scaled by column. Averages shown for *N* = 3–9 mice. **(G)** Total number of live cells. **(H)** Representative FACS plot of percent neutrophils (CD11b+Ly6G+) of CD45$^+$ live cells and quantification. **(I)** Percent neutrophils of total live cells. **(J)** Total number of live neutrophils. Data in F–J were pooled from independent experiments. **(K)** Intradermal *S. aureus* infection (USA300 LAC strain with *agrI* YFP reporter) model used with *Pdgfra*$^{\Delta Il17ra}$ and Cre− littermates (control) in L–O. The experiment was performed five times with *N* = 3–6 mice per independent experiment ending on day 5 and *N* = 4 mice per independent experiment ending on day 2. **(L)** Expression of neutrophil chemokines, proinflammatory cytokines, and other host defense genes on day 2 by qPCR, scaled by column. Averages are shown for *N* = 3–4 mice. Naïve mouse data are the same as in F. **(M)** Representative GR-1 (neutrophils) immunostaining on day 2. Scale bar, 300 µm. **(N and O)** (N) Representative in vivo day 2 images of *S. aureus* reporter expression and quantification and (O) representative day 1 images of lesions and size quantification (*N* = 8–13 mice). Scale bars, 10 mm for N and 2 mm for O. Data in N–O were pooled from independent experiments. Error bars represent SEM. ns (not significant), **P < 0.01, ***P < 0.001, and ****P < 0.0001 using unpaired *t* test.

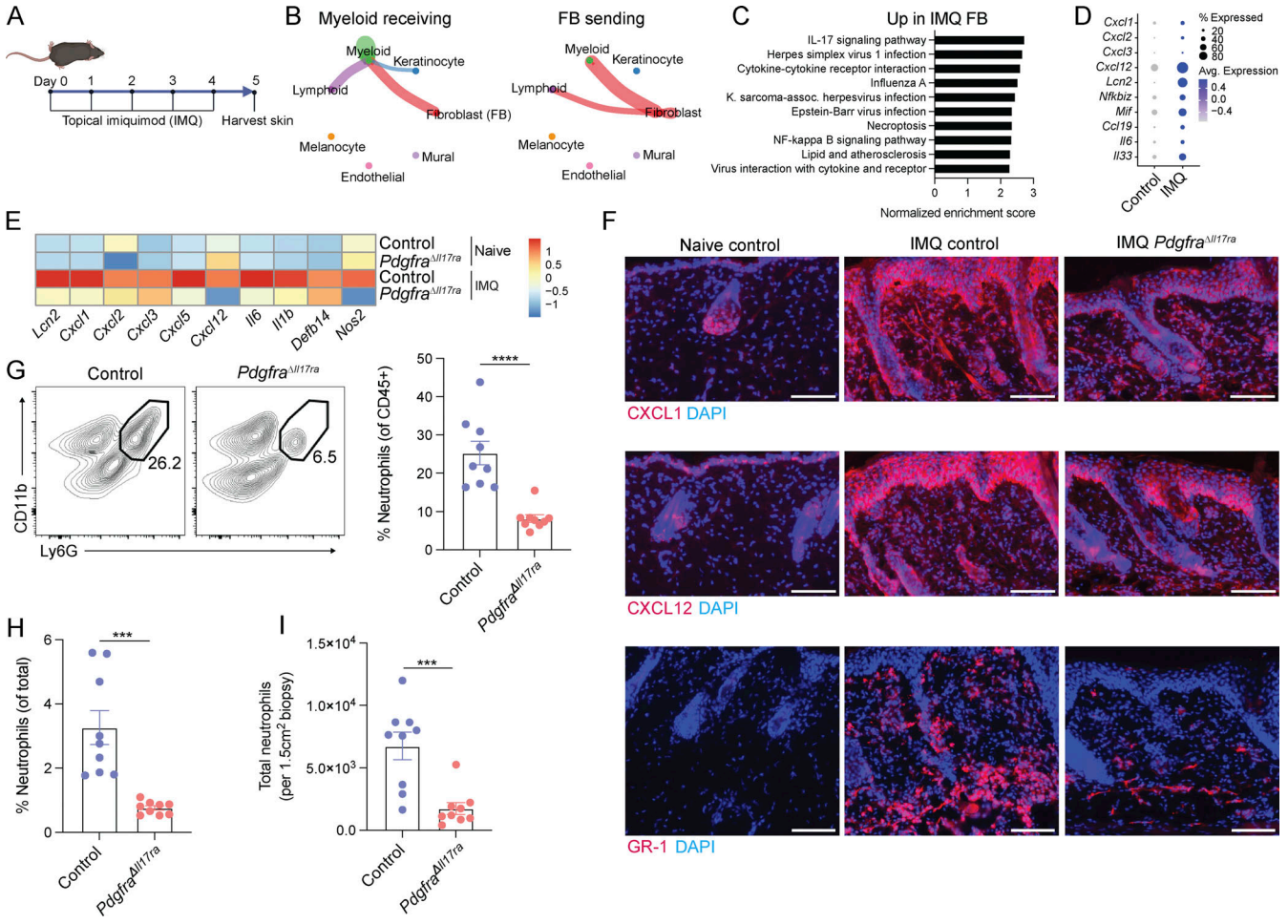


Figure 5. **Fibroblast IL-17 signaling is required for neutrophil skin inflammation in an IMQ-induced psoriasis model. (A)** Schematic of IMQ induced psoriasis model. **(B–D)** scRNA-Seq using back skin from WT mice treated with IMQ or vehicle (control). Data were obtained from samples pooled from *N* = 4 mice independently treated in each group. **(B)** Network analysis showing communication toward myeloid cells (left) and from fibroblasts (right). Edge weight is proportional to communication strength. Edge and node color indicates communication source. **(C)** GSEA of fibroblast using KEGG database. **(D)** Expression of host defense genes in fibroblast. **(E–J)** IMQ model in *Pdgfra*-Cre × *Il17ra* fl/fl (*Pdgfra*$^{\Delta Il17ra}$) and Cre− littermates (control). The experiment was performed three times with *N* = 2–4 mice per independent experiment. **(E)** Expression of neutrophil chemokines, proinflammatory cytokines, and other host defense genes by qPCR, scaled by column. Averages shown for *N* = 3–5 mice. Naïve mouse data are the same as in Fig. 4 F. **(F)** Representative immunostaining for CXCL1, CXCL12, and GR-1 (neutrophils). Scale bar, 150 µm. **(G)** Representative FACS plot of percent neutrophils (CD11b+Ly6G+) of CD45$^+$ live cells and quantification. **(H)** Percent neutrophils of total live cells. **(I)** Total number of live neutrophils. Data in G–I were pooled from independent experiments. Error bars represent SEM. ***P < 0.001, and ****P < 0.0001 using unpaired *t* test.

are involved in psoriasis, a human disease characterized by type 17 inflammation and responsive to drugs targeting IL-17 and TNFα signaling (Hong et al., 2022). scRNA-Seq analysis of lesional psoriasis skin was compared with healthy skin (Fig. 6 A) (Gao et al., 2021). Major cell lineages recovered were identified as fibroblasts, keratinocytes, myeloid cells, lymphoid cells, mural cells, melanocytes, endothelial cells, and Schwann cells based on marker gene expression (Fig. S5 K). As in our mouse models, network analysis of skin affected by psoriasis showed strong fibroblast-to-myeloid communication (Fig. 6 B). Psoriasis dermal fibroblasts upregulated genes consistent with IL-17 signaling (Fig. 6 C) and expressed neutrophil chemokines including *CXCL1* and *CXCL12* at levels greater than other cell lineages (Fig. 6 D).

Unsupervised clustering of the fibroblast subset resolved 11 clusters with unique expression of marker genes (Fig. 6 E and Fig. S5 L). Plotting expression of known markers for papillary, reticular, adipocyte lineage, and myofibroblast subsets (Table S1) identified FB1–FB6 as reticular and adipocyte lineage clusters and FB7–FB11 as papillary and myofibroblast clusters, respectively (Fig. 6 F). Unbiased differential expression and pathway analysis confirmed this finding and revealed that reticular and adipocyte lineage cells highly expressed genes important for communication with neutrophils ("neutrophil migration"), whereas papillary and myofibroblasts highly expressed genes important for producing matrix ("skin development") and fibrosis ("Wnt signaling pathway") (Fig. 6, G and H). Indeed, expression of neutrophil chemokines *CXCL1*, *CXCL2*, *CXCL3*, *CXCL5*, *CXCL8*, and *CXCL12* was enriched in FB1–FB6 (Fig. 6 I). Notably, individual clusters expressed unique profiles of neutrophil chemokines. For example, *CXCL12* was broadly expressed across FB1–FB6, whereas *CXCL3* was observed primarily in FB3. To specifically characterize human neutrophil-recruiting dermal

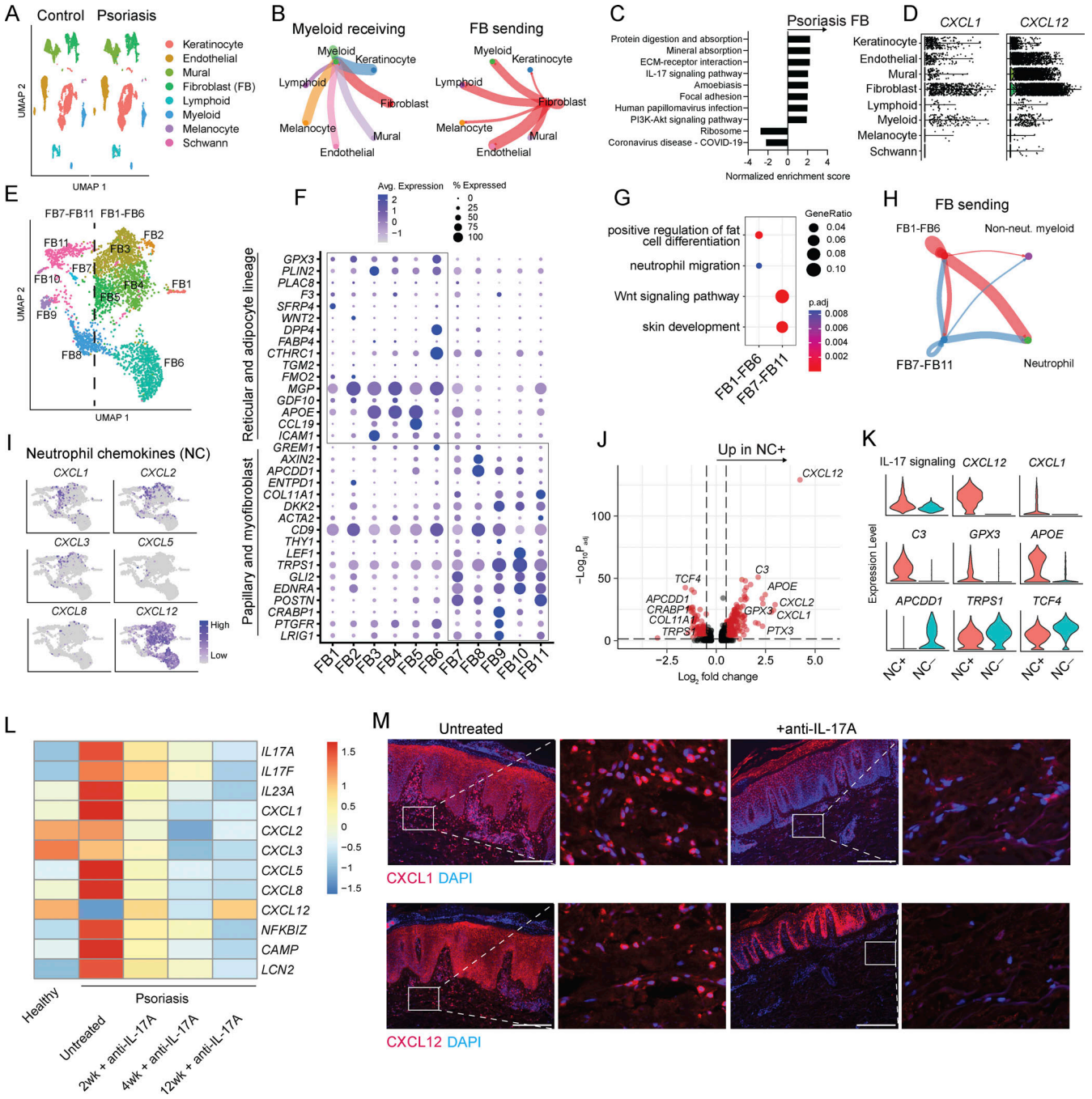


Figure 6. **scRNA-Seq of human skin reveals IL-17–mediated CXCL12+ dermal fibroblast–neutrophil communication in psoriasis. (A–K)** Analysis of scRNA-Seq of skin from psoriasis patients ($N$ = 3) and healthy controls ($N$ = 3). **(A)** Dimensionality reduction is split by condition and colored by cell type. **(B)** Network analysis showing communication toward myeloid cells (left) and from fibroblasts (right). Edge weight is proportional to communication strength. Edge and node color indicates communication source. **(C)** GSEA of fibroblasts using KEGG database. **(D)** Expression of neutrophil chemokines across cell types. **(E)** Dimensionality reduction of fibroblast subset colored by cluster. Dashed line separates FB1–FB6 and FB7–FB11. **(F)** Expression of fibroblast subset marker genes across clusters. Boxes highlight high expression of reticular and adipocyte lineage genes in FB1–FB6 and high expression of papillary and myofibroblast genes in FB7–FB11. **(G)** GO term analysis comparing FB1–FB6 and FB7–FB11. **(H)** Network analysis showing communication from FB1–FB6 and FB7–FB11 toward neutrophils and other myeloid cells. **(I)** Neutrophil chemokine expression across fibroblast clusters. **(J)** DEGs between neutrophil chemokine+/− fibroblasts in psoriasis using Wilcoxon Rank Sum test. $Log_2$ fold-change and P value (adjusted) cut-offs are 0.5 and 0.05, respectively. **(K)** Expression of neutrophil chemokine+/− fibroblast markers in psoriasis. **(L)** Expression of genes associated with fibroblast–neutrophil communication by bulk RNA-Seq in human psoriasis patients on and off anti–IL-17A treatment, scaled by row. Averages shown for $N$ = 8–10. **(M)** Representative CXCL1 and CXCL12 immunostaining in lesional skin from psoriasis patients untreated and treated with anti–IL-17A. Scale bar, 300 µm.

fibroblasts, we classified fibroblasts in psoriasis as neutrophil chemokine+ (defined as expressing *CXCL1*, *CXCL2*, *CXCL3*, *CXCL5*, *CXCL8*, or *CXCL12*) or neutrophil chemokine− (defined as lacking *CXCL1*, *CXCL2*, *CXCL3*, *CXCL5*, *CXCL8*, and *CXCL12* expression) and found that 83% of neutrophil chemokine+ cells belonged to reticular and adipocyte lineage clusters FB1–FB6 and 17% belonged to papillary and myofibroblasts clusters FB7–FB11 (Fig. S5, M and N). As in mice, differential expression analysis between neutrophil chemokine+ and neutrophil chemokine− fibroblasts indicated that *CXCL12* was a highly sensitive and specific marker of human neutrophil chemokine+ fibroblasts (Fig. 6, J and K).

To determine the significance of IL-17 signaling in CXCL12+ dermal fibroblasts in humans, we analyzed transcriptomic data from healthy controls and psoriasis patients undergoing anti–IL-17 treatment (Liu et al., 2021) (Fig. 6 L). This analysis confirmed that the expression of neutrophil chemokines and other host defense genes was increased in psoriasis in an IL-17–dependent manner. A role for IL-17 signaling in the induction of CXCL1 and CXCL12 by dermal fibroblasts specifically was supported by immunofluorescence of human skin biopsies from psoriasis patients: more intense dermal staining of CXCL1 and CXCL12 and inflammation was observed in untreated psoriasis compared with psoriasis treated with anti–IL-17A (Fig. 6 M and Fig. S5 O).

## Discussion

In this study, we sought to obtain a more comprehensive understanding of the cell–cell interactions underlying cutaneous host defense and focused first on the skin response against *S. aureus*, the major pathogen of deep tissue infections in humans (Miller and Cho, 2011). Unbiased network analysis of single-cell transcriptomic data during infection of mice showed that CXCL12+ adipocyte lineage subsets of dermal fibroblasts served as the dominant hub for communication with neutrophils. Furthermore, subsequent functional analysis in vitro and in mice demonstrated that these fibroblasts are important for recruiting neutrophils and mounting an effective host defense response. Thus, our data provide direct evidence that the inflammatory neutrophil defense response of the skin initiated by recognition of IL-17 is mediated by some dermal fibroblasts and suggests that these dermal stromal cells contribute to both infectious and non-infectious forms of skin inflammation. Although prior models of cutaneous host defense have focused on the roles of epithelial keratinocytes, resident dendritic cells, mast cells, macrophages, lymphocytes, and endothelia (Miller and Cho, 2011; Moos et al., 2023), these prior models failed to recognize that immune acting fibroblasts (IAFs) play a pivotal role in the innate immune response of the skin. Our findings now show that CXCL12+ fibroblasts within the mixed fibroblast community in the skin serve a key role in neutrophil recruitment during type 17 inflammation.

Dermal fibroblasts are heterogenous and can be grouped into two major lineages: an upper, epidermis-adjacent lineage that gives rise to papillary fibroblasts, and a lower lineage that gives rise to reticular fibroblasts and adipocytes (Driskell et al., 2013). Dermal FfibroblastsBs are not strictly spatially distributed as cells exhibiting a profibrotic myofibroblast phenotype can be found in both the upper and lower levels of the dermis (Janson et al., 2012), and perifollicular fibroblasts and mural cells likely represent unique states of fibroblast differentiation. Our group previously showed that *S. aureus* infection induces dermal fibroblasts in a preadipocyte lineage to differentiate into mature adipocytes and secrete the antimicrobial peptide CRAMP (Zhang et al., 2015). Thus, it was of interest to further study the potential functions of dermal fibroblasts during different forms of skin inflammation.

Single-cell transcriptomics led to the identification that CXCL12+ dermal fibroblast subsets, marked by reticular and adipocyte lineage genes, can play a role in communication with neutrophils and antimicrobial defense without maturation into adipocytes. Confocal microscopy confirmed that CXCL12+ fibroblasts reside primarily in the reticular dermis. Single-cell transcriptomics of skin from patients with psoriasis, a non-infectious inflammatory skin disease, further found that analogous human CXCL12+ subsets of IAFs express neutrophil chemokines, an observation in line with a 2023 study identifying that some dermal fibroblasts in psoriasis express high levels of proinflammatory genes and low levels of extracellular matrix genes (Ma et al., 2023). Both human and mouse CXCL12+ dermal fibroblast subsets were marked by high expression of neutrophil chemokines (CXCR2 ligands), complement factor C3, and reticular marker GPX3, and low expression of papillary marker APCDD1 and myofibroblast markers TRPS1 and TCF4. Distinctions were, however, noted between mouse and human CXCL12+ IAFs. For example, IFI205, PLAC8, and LPL marked mouse but not human cells, and APOE marked human but not mouse cells. Taken together, our new observations distinguish between previously unknown CXCL12+ subsets of dermal fibroblasts with important immune defense activity and different CXCL12− subsets of dermal fibroblasts that largely exist in the papillary dermis and appear to serve matrix-producing functions. We hypothesize that CXCL12+ IAFs are themselves diverse and plastic, providing a dynamic resident cell population in the dermis that serves to amplify inflammatory responses.

GSEA of single-cell transcriptomic data from infectious and non-infectious neutrophil-laden mouse and human skin revealed that CXCL12+ dermal fibroblast subsets expressed genes consistent with IL-17 signaling. IL-17–producing lymphocytes including Th17 cells, γδT cells, and group 3 innate lymphoid cells orchestrate neutrophil recruitment to numerous tissues for host defense. In the skin, mice deficient in γδT cells or IL-17RA have been shown to have impaired neutrophil recruitment following i.d. *S. aureus* infection, leading to more bacterial growth and lesion development (Cho et al., 2010). IL-17 also promotes neutrophil inflammation in several autoinflammatory conditions such as psoriasis, and biologics targeting the IL-17 pathway are highly effective in treating patients with these diseases but increase the risk of infection (Liu et al., 2021). Using in vitro studies with Th17 cells and recombinant cytokines, we found that IL-17 induced upregulation of neutrophil chemokines in CXCL12+ fibroblasts. When IL-17 was combined with other TLR ligands and proinflammatory cytokines involved in host defense against *S. aureus*, synergistic activation was observed—especially when IL-17 was combined with TNFα. Notably, the

activation program induced by IL-17 and TNFα was distinct from that induced by the initiation of adipogenesis: IL-17 and TNFα drove the expression of a broad array of antimicrobials, chemokines, and proinflammatory cytokines, whereas adipogenesis induced only a few host defense genes like *Camp* and *Lcn2*.

Using a combination of transcriptomic and multiplex protein assays, we found that in vitro stimulation with IL-17A and TNFα induced CXCL12+ preadipocyte fibroblast upregulation of numerous antimicrobials, cytokines, and chemokines. We subsequently found using transwell migration assays that activated CXCL12+ preadipocyte fibroblasts drove robust neutrophil migration and some monocyte and lymphocyte migration. Neutrophil migration was completely dependent on ligands for CXCR2 (CXCL1, CXCL2, CXCL3, and CXCL5) and CXCR4 (CXCL12), demonstrating that CXCL12 is also a functional marker of IAFs. Our in vitro experiments also identified the NF-κB cofactor NFKBIZ as a key transcription factor regulating CXCL12+ preadipocyte fibroblast production of neutrophil chemokines and neutrophil recruitment. These findings are supported by another study showing that synovial fibroblasts from patients with rheumatoid arthritis promoted NFKBIZ-dependent neutrophil migration (Slowikowski et al., 2020).

To demonstrate the significance of CXCL12+ dermal fibroblast–neutrophil communication in vivo, we chose to selectively delete from fibroblasts IL-17RA, a factor we showed to be upstream of neutrophil chemokine production. This approach was chosen because we found that dermal fibroblasts activated by IL-17 secrete many neutrophil chemokines. However, there are some limitations to this approach. First, it did not allow us to determine the requirement for specific chemokines, though our in vitro experiments suggest CXCR2 and CXCR4 ligands are key. Second, other IL-17RA ligands, including IL-17E, IL-17B, and IL-17C, may have contributed to the observed phenotype in addition to IL-17A/F; however, this is highly unlikely as MDFBs were shown to lack expression of the necessary coreceptors IL-17RB and IL-17RE. Finally, it does not rule out alternative, indirect mechanism(s) underlying the changes in neutrophil recruitment we observed in vivo. For example, it is possible that IL-17 could activate fibroblasts to produce proinflammatory cytokines that activate other cells like myeloid cells and keratinocytes to produce neutrophil chemokines. Nevertheless, our results conclusively demonstrate that IL-17 activates fibroblasts to enable neutrophil recruitment to the skin. This observation is also consistent with a 2021 study that found that lung fibroblast recognition of IL-17 was critical for vaccination against *Klebsiella pneumoniae* (Iwanaga et al., 2021), suggesting that similar fibroblast subsets may play a role in host defense in the lung.

Our study has important clinical implications. Monoclonal antibodies targeting IL-17 and TNFα are highly effective in treating patients with psoriasis and other neutrophilic dermatoses (Rodríguez-Cerdeira et al., 2021; Kimball et al., 2023). Our comprehensive mouse and human in vitro and in vivo work reveal that one important mechanism by which these biologics work may be through the inhibition of CXCL12+ dermal fibroblast communication with neutrophils. Notably, there are downsides to these drugs including high cost, increased risk of infection, efficacy in only a subset of patients, and loss of efficacy over time. By improving the understanding of how IL-17 and TNFα inhibitors work, our findings can serve as the basis for the design of therapeutics that are more effective and affordable and have fewer side effects. In addition to skin infection and psoriasis, there are many other IL-17– and TNF-mediated diseases that afflict large numbers of patients and remain inadequately treated including but not limited to neutrophilic dermatoses, neutrophilic asthma, and inflammatory bowel disease. The role of IL-17– and TNF-mediated fibroblast–neutrophil communication is unknown in these diseases and should be investigated to better understand pathogenesis and improve treatment.

In summary, our work here illuminates a previously unrecognized and important role for some subsets of dermal fibroblasts in neutrophil recruitment to the skin that should be incorporated into models of cutaneous host defense and inflammation. This work provides insight into the mechanisms underlying the clinical success of biologics targeting IL-17 and TNFα and identifies CXCL12+ IAF-neutrophil communication as a novel therapeutic target for the treatment of skin diseases including bacterial infection and psoriasis.

## Materials and methods

### Study design

The aim of this study was to understand the cellular and molecular mechanisms underlying host defense against cutaneous *S. aureus* infection. To this end, we performed scRNA-Seq with unbiased network and pathway analysis and identified IL-17–mediated fibroblast-to-neutrophil communication as a potential mechanism. In vitro studies were used to model lymphocyte–fibroblast–neutrophil interactions. To demonstrate the significance of these mechanisms, we developed conditional knockout mice lacking *Il17ra* specifically in fibroblasts. Patients with psoriasis on and off anti–IL-17 treatment were recruited for a skin biopsy to translate findings to humans.

### Animals and animal care

All animal experiments were approved by the University of California, San Diego (UCSD) Institutional Animal Care and Use Committee. WT C57BL/6 mice were purchased from The Jackson Laboratory. *Camp*$^{-/-}$, *Lcn2*$^{-/-}$, *Tnfrsf1a*$^{-/-}$, *Pdgfra*-Cre, and *Il17ra*-fl/fl mice on C57BL/6 background were purchased from The Jackson Laboratory and bred and maintained at UCSD. Mice were housed under a specific pathogen–free condition with 12-h light and 12-h dark cycle at 20–22°C and 30–70% humidity. Experimental and littermate control animals were age- and sex-matched 7–9-wk-old males and females.

### Human skin sample collection

Human lesional skin biopsies from the right elbow of 30–50-yr-old male psoriasis patients were collected from the Dermatology Clinic, UCSD. Sample acquisitions were approved and regulated by the UCSD Institutional Review Board (140144). Written informed consent was obtained from all subjects. Biopsies were immediately embedded in OCT compound (4583; Sakura) for sectioning and staining.

### Mouse models

1–3 days prior to experiments, mice were randomly selected, and back skin was shaved, treated with depilatory cream (Nair), and rinsed with water. For *S. aureus* skin infection, 5e6 CFU mid-logarithmic growth phase strain USA300 LAC *agrI* P3-YFP (cmR) AH1677 was injected i.d. in 50 µl PBS. YFP expression was monitored on days 0, 1, 2, and 5 using an IVIS Spectrum (Perkin Elmer) with autoexposure settings. In some experiments, the skin was harvested on day 2 for qPCR. For recombinant cytokine-induced neutrophil recruitment, 500 ng rmIL-17A (317-ILB-050; R&D) and/or 200 ng rmTNFα (PMC3014; Thermo Fisher Scientific) was injected i.d. in 50 µl PBS daily for three consecutive days. Skin was harvested 24 h after the third challenge for qPCR, flow cytometry, and immunofluorescence. A blinded individual was assigned gross inflammation scores, with 0 being no inflammation and 5 being severe inflammation. For IMQ-induced psoriasis-like inflammation, 5% IMQ (51672414506; McKesson Medical Surgical) or control cream (56614-414; VWR) was applied topically on back skin daily for 5 days. Skin was harvested 24 h after the fifth challenge for qPCR, flow cytometry, and immunofluorescence.

### scRNA-Seq

Four biopsies from biological replicates were pooled per condition. Single-cell suspensions were generated by mechanical digestion followed by enzymatic digestion in Hanks' balanced salt solution (#14175095; Thermo Fisher Scientific) supplemented with bovine serum albumin (20 mg/ml), antibiotic–antimycotic (#15240062; Thermo Fisher Scientific), deoxyribonuclease I (50 U/ml; #04716728001; Sigma-Aldrich), liberase (0.1 mg/ml; #05401020001; Sigma-Aldrich), Hepes (20 mM, #15630080; Thermo Fisher Scientific), sodium pyruvate (2 mM, #11360070; Thermo Fisher Scientific), and collagenase type IV (1 mg/ml; #17104019; Thermo Fisher Scientific) for 45 min at 37°C with constant rotation. Enzymatic dissociation was terminated by the addition of 5 mM EDTA and 10% FBS. Digests were filtered twice through a 40-µm filter, followed by the removal of dead cells using the MACS Dead Cell Removal Kit (130-090-101; Miltenyi Biotec). Libraries were generated using 10X Genomics 3′ V3.1 protocol with 16,000 cells loaded per sample and sequenced on a Novaseq 6000 (Illumina). Cell Ranger (10X Genomics) with default parameters was used to perform sample demultiplexing, barcode processing, alignment to the mm10 reference genome, and gene counting. Data were filtered, processed, and analyzed using Seurat. All functions described below are Seurat functions unless stated otherwise. Filtering data involved selecting cells with >200 features, >300 unique molecular indicators, and <10% mitochondrial genes, removing ambient RNA with SoupX with setContaminationFraction = 0.2 (Young and Behjati, 2020) and doublets using DoubletFinder with the default settings (McGinnis et al., 2019). Data were normalized and integrated using NormalizeData and IntegrateData with default parameters. Clusters were identified using FindNeighbors with 50 principal components and FindClusters with a range of resolutions. For each resolution, nonlinear dimensionality reduction and visualization were performed with 50 principal components, and marker genes for each cluster were determined using FindAllMarkers with min.pct = 0.25. The resolution yielding clusters with the most distinct marker genes were chosen for further analysis. For fibroblast and myeloid subset analysis, data were subset based on marker genes, contaminating cells were removed, and the above analysis was repeated. GSEA and overrepresentation analysis were performed using ClusterProfiler (Yu et al., 2012) and network analysis was performed using CellChat (Jin et al., 2021). IL-17 signaling score was quantified using AddModuleScore with genes identified using ClusterProfiler (mouse: *Cxcl1*, *Il6*, *Cxcl2*, *Ptgs2*, *Cxcl5*, *Csf3*, *Lcn2*, *Mmp3*, *Ccl2*, *Vav3*, *Bcl2*, *Vegfa*, *Ctsk*, *Cxcl12*, *Nos2*, and *C4b*; human: *CXCL1*, *CXCL2*, *CXCL3*, *CXCL8*, *IL6*, *TRAF3*, *TBK1*, *PTGS2*, *CEBPB*, *MMP1*, *HSP90B1*, *NFKB1*, *NFKBIA*, *CCL2*, *TNFAIP3*, and *FOSB*).

### RNA isolation, cDNA library preparation, and RT-qPCR

RNA from cells and tissues were preserved with RNAlater (AM7020; Thermo Fisher Scientific). In select experiments, the epidermis and dermis were enzymatically separated prior to RNA preservation by overnight incubation in Dispase (10 mg/ml, D4693; Sigma-Aldrich). Samples were lysed and RNA was isolated using PureLink Isolation kit (12183025; Thermo Fisher Scientific) and made into cDNA using Verso cDNA synthesis kit (AB1453/B; Thermo Fisher Scientific). qPCR was performed using the CFX96 Real-Time System (Bio-Rad) with SYBR Green Mix (QP1311; Biomiga). Housekeeping genes *Tbp* and *TBP* were used to normalize expression for mice and humans, respectively. Specific primer sequences (IDT) are shown in Table S2. Heatmaps were generated using average values with pheatmap. Top variable genes between groups for heatmaps were identified using the R function rowVars().

### Histology and immunofluorescence

Skin biopsies were embedded fresh in OCT, frozen, and sectioned to 20 µm at −20°C using a Leica CM1860 cryostat. Skin sections or cells grown in chamber slides were briefly fixed in 4% paraformaldehyde, blocked with serum from secondary antibody host, stained with primary antibodies overnight at 4°C, secondary antibodies for 1 h at room temperature, and nuclei were counterstained with DAPI. Epifluorescence images were taken using an EVOS5000, and confocal images were taken on a Nikon A1R. Brightness and contrast were adjusted slightly using ImageJ or Nikon elements software and applied equally across samples. Primary antibodies were as follows: PDGFRα (1:200, 14-1401-82; eBioscience), CRAMP (made in house, 1:100), LCN2 (1:100, AF1757; R&D), GR-1 (1:100, 108435; BioLegend), CXCL1 (1:100, PA586508; Thermo Fisher Scientific), CXCL12 (1:1,000, 14-7992-81; Thermo Fisher Scientific), MOMA-2 (1:100, MCA519G; Bio-Rad), and p65 (1:1,000, 8242; Cell Signaling Technologies). Secondary antibodies were as follows: Alexa Fluor 488 AffiniPure Donkey Anti-Rat IgG (H+L) (1:100, 712-545-153; JacksonImmunoResearch), Rhodamine Red-X AffiniPure Donkey Anti-Rabbit IgG (H+L) (1:100, 711-295-152; JacksonImmunoResearch), Cy3 Donkey anti-Rabbit IgG (1:500, 406402; BioLegend), Donkey anti-Rat IgG (H+L) Highly Cross-Adsorbed Secondary Antibody, Alexa Fluor 488 (1:1,000, A21208; Thermo Fisher Scientific), and Cy3 Goat anti-Rat IgG (1:500, 405408; BioLegend).

### Cell culture

All cells were grown in a humidified incubator at 5% $CO_2$ and 37°C under sterile conditions. Th17 CM was generated using the CellXVivo Mouse Th17 Cell Differentiation Kit (CDK017; R&D) according to the manufacturer's instructions with a naïve T cell isolation kit (130-104-453; Miltenyi Biotec). IL-17A was blocked using anti–IL-17A (BE0173; BioXcell, 20 µg/ml). 3T3-L1 mouse preadipocyte fibroblasts were purchased from the American Type Culture Collection (CL-173) and used prior to passage 10. For primary fibroblast studies, neonatal (P1) cells were used unless otherwise noted. Primary dermal fibroblasts were isolated by our laboratory as previously described (Zhang et al., 2019) and used in passage 1. Cells were grown in Dulbecco's Modified Eagle Medium (DMEM) supplemented with 10% FBS, Glutamax (35050061; Thermo Fisher Scientific), and antibiotic–antimycotic (15240062; Thermo Fisher Scientific). 2-day post-confluent cells were stimulated with recombinant cytokines, purified toll ligands, or an adipogenesis-inducing cocktail. Adipogenesis was induced as described previously (Zhang et al., 2015). Cells were assayed at 24 h for qPCR, RNA-Seq, and flow cytometry, and at 72 h for western blot, immunofluorescence, and CM experiments. Recombinant cytokines and purified toll ligands used include rmIL-17A (50 ng/ml, 421-ML-100/CF; R&D), rhIL-17A (50 ng/ml, 317-ILB-050; R&D), rmTNFα (20 ng/ml, PMC3014; Thermo Fisher Scientific), rhTNFα (20 ng/ml, 210-TA-020/CF; R&D), rmIL-17F (50 ng/ml, 2057-IL-025; R&D), MALP2 (100 ng/ml, ALX-162-027-C050; Enzo), rmIL-1β (10 ng/ml, 50101-MNAE; SinoBiological), Pam3CSK4 ( 0.2 µg/ml, TLRL-PMS; Invivogen), FSL-1 (0.2 µg/ml, TLRL-FSL; Invivogen), LPS (0.5 µg/ml, TLRL-PB5LPS; Invivogen), FLA-ST (0.2 µg/ml, TLRL-STFLA; Invivogen), Poly(I:C) (2 µg/ml, TLRL-PICW; Invivogen), IMQ (0.2 µg/ml, TLRL-IMQS; Invivogen), and ODN2395 (TLRL-2395, 1 µM). In some experiments, fibroblasts were treated with pharmacological inhibitors against JNK (30 µM, SP600125; Sigma-Aldrich), P38 MAPK (10 µM, SB203580; Invivogen), and JAK (1 µM, PZ0017; Sigma-Aldrich).

### siRNA knockdown

siRNA knockdown was performed on 1-day post-confluent cells. Transfection was performed using RNAi Max Lipofectamine (13778075; Thermo Fisher Scientific) and OptiMEM (31985-062; Thermo Fisher Scientific) according to the manufacturer's protocol. Pooled siRNAs (Dharmacon) were used at 30 nM and included scramble control (D-001810-10-05), *Nfkbiz* (L-040680-00-0005), *Tnfrsf1a* (L-060201-01-0005), *Tnfrsf1b* (L-043973-00-0005), *Cxcl2* (L-044397-00-0005), and *Hif1a* (L-040638-00-0005).

### RNA-Seq

Isolated RNA passing quality control (RNA integrity number > 8) underwent stranded mRNA sequencing on a Novaseq 6000 (Illumina) with paired-end 100 base-pair reads. Reads were aligned to reference genomes (mm10 and hg38) using STAR (Dobin et al., 2013), and count tables were generated using FeatureCounts (Liao et al., 2019). Variance stabilization transformation normalization and differential expression analysis were performed using DESeq2 (Love et al., 2014). Heatmaps were generated using average value with pheatmap. Top variable genes between groups for heatmaps were identified using the R function rowVars(). Overrepresentation pathway analysis was performed using ClusterProfiler (Yu et al., 2012).

### Western blot

Fibroblasts were lysed in radioimmunoprecipitation assay buffer (R3792; Teknova) with protease inhibitor (78440; Thermo Fisher Scientific). Protein levels of lysates were quantified using bicinchoninic acid assay (23225; Thermo Fisher Scientific). 15 µg of lysate was mixed with Laemmli sample buffer (1610747; Bio-Rad) supplemented with 2-mercaptoethanol, and CM was mixed with loading dye (LC1676; Invitrogen) and reducing agent (NuPAGE Sample Reducing Agent, 10X). Samples were incubated at 80°C for 5 min. Lysate was loaded into a 4–12% Bis-Tris gel (NP0323BOX; Invitrogen) and CM was loaded into a 10–20% tricine gel (EC66252BOX; Invitrogen). Gels were transferred to polyvinylidene fluoride membranes using Trans-Blot Turbo Transfer Pack (1704156; Bio-Rad) according to the manufacturer's instructions. Membranes were blocked with TBS-based Odyssey blocking buffer (927-60001; LI-COR) and incubated overnight at 4°C with primary antibodies from Cell Signaling Technologies diluted to 1:1,000. These included p65 (8242), phospho-IκBα (9246S), phospho-IKKα/β (2078S), phospho-p105 (4806S), and phospho-p65 (3039). Membranes were washed and incubated with fluorescent secondary antibodies (LI-COR) for 1 h at room temperature and imaged using an Odyssey Infrared Imager (LI-COR).

### ELISA

ELISAs for CXCL12 (R&D, MCX120) and CXCL8 (R&D, DY208) were performed according to the manufacturers' protocols and read on a DTX880 plate reader (Beckman Coulter) at 450 nm.

### Multiplex immunoassay

The multiplex immunoassay was performed on fibroblast CM using LEGENDplex Mouse Proinflammatory Chemokine Panel (13-plex) with Filter Plate (740007; BioLegend) according to the manufacturer's protocol. Samples were read using a Novocyte (ACEA) flow cytometer. Heatmaps were generated using average values with pheatmap.

### Flow cytometry

Single-cell suspensions were prepared as described above. Cells were incubated with anti-CD16/CD32 (101302; BioLegend) for 10 min at 4°C to block non-specific Fc receptor binding and then incubated for 30 min with fluorochrome-conjugated antibodies diluted to 1:50 at 4°C including anti-Ly6G (127608; BioLegend), anti-CD11b (101212; BioLegend), and anti-CD45 (109828; BioLegend). For fibroblast intracellular cytokine staining, cells were incubated for 24 h at 37°C with proinflammatory cytokines in complete media supplemented with a protein transport inhibitor cocktail (00-4980-93; Thermo Fisher Scientific). Stimulated cells were harvested, fixed, and permeabilized (00-5523-00; Thermo Fisher Scientific), and then stained with anti-CXCL1 (IC4532R; R&D). Cell counting and flow cytometric acquisition was performed using a Novocyte (ACEA) flow cytometer. Data were analyzed using FlowJo (BD).

### Neutrophil migration and activation assays

Bone marrow was flushed from femurs and tibias of WT mice. Following red blood cell lysis, samples were filtered through a 40-µm strainer and resuspended at 2e6 cells/ml in DMEM with 0.5% FBS. 200 µl of the bone marrow suspension was loaded into the upper chamber of each well in a 3-µm 24-well transwell plate. 600 µl of fibroblast CM (0.5% FBS) was loaded into the bottom chamber. Cells were allowed to migrate for 3 h at 37°C. After 3 h, 60 µl 0.5 M EDTA was added to lower chambers and plates were incubated at 4°C for 15 min. Migrated cells were collected from the lower chamber, counted, and stained for flow cytometric analysis as described above. In some experiments, purified neutrophils were used in place of bone marrow leukocytes. In some experiments, fibroblast CM or bone marrow cells were preincubated for 30 min at 4°C with pharmacological inhibitors targeting MIF (1 µM, 475837; Calbiochem), pertussis toxin (1 µg/ml, PHZ1174; Thermo Fisher Scientific), CXCR4 (10 µg/ml, ab120718; Abcam), and CXCR2 (1 µM, Sch527123; Calbiochem). For neutrophil activation assays, 750,000 purified neutrophils/ml were incubated for 3 h in fibroblast CM prior to qPCR and bulk RNA-Seq.

### Statistical analysis

Unless indicated otherwise, experiments were performed with at least biological triplicates and repeated at least twice. Statistical significance was calculated using R or GraphPad Prism with *P < 0.05, **P < 0.01, ***P < 0.001, and ****P < 0.0001. For more information, please see figure legends.

### Study approval

All animal experiments were approved by the UCSD Institutional Animal Care and Use Committee (#S09074). For human studies, all sample acquisitions were approved by the UCSD Institutional Review Board (#140144).

### Online supplemental material

Fig. S1 shows additional scRNA-Seq analysis of i.d. *S. aureus* infection, neutrophil kinetics during i.d. *S. aureus* infection, and scRNA-Seq analysis of topical *S. aureus* infection. Fig. S2 shows 3T3-L1, MDFB, and HPAD response to TLR ligands and proinflammatory cytokines. Fig. S3 shows 3T3-L1 response to IL-17 and TNF with genetic and pharmacological inhibition of signaling intermediates. Fig. S4 shows the effect of fibroblast CM on neutrophil activation and leukocyte migration. Fig. S5 shows fibroblast expression of IL-17 receptors, fibroblast conditional knockout validation, the significance of fibroblast IL-17 signaling in recombinant cytokine injection and topical IMQ models, IMQ-induced chemokine expression in dermis versus epidermis, additional analysis of mouse IMQ and human psoriasis scRNA-Seq, and H&E of skin from psoriasis patients on and off anti–IL-17A. Table S1 shows fibroblast subset markers. Table S2 shows RT-qPCR primers.

### Data availability

Genomic data presented here are available in the National Center for Biotechnology Information Gene Expression Omnibus database under reference series GSE230513.

## Acknowledgments

We thank Romana Gerner and Manuela Raffatellu (UCSD) for generously providing the *Lcn2*$^{-/-}$ mice, Alexander Horswill for providing the *S. aureus* reporter strain, and Taylor Doherty and David Broide (UCSD) for flow cytometry resources. This publication includes data generated at the UCSD Institute for Genomic Medicine Genomics Center with the help of Kristen Jepsen utilizing an Illumina NovaSeq 6000 that was purchased with funding from a National Institutes of Health Shared Instrumentation Grant (#S10 OD026929) and data generated at the UCSD Cancer Center Microscopy Shared Facility with the help of Kersi Pestonjamasp utilizing equipment that was purchased with funding from a Specialized Support Grant P30 (CA23100-28). Figure models were created using https://BioRender.com.

K.J. Cavagnero is supported by National Science Foundation GRFP2038238 and National Institutes of Health (NIH) T32DK007202, and R.L. Gallo is supported by NIH R01DK121760, NIH R01AR076082, NIH R01AI153185, U01AI152038, P50AR080594, and NIH R37AI052453.

Author contributions: K.J. Cavagnero—conceptualization, investigation, resources, software, formal analysis, visualization, writing (original draft), writing (review & editing); C. Aguilera, O. Osuoji, and T. Hata—resources; F. Li, T. Dokoshi, T. Nakatsuji, A. O'Neill, E. Liu, and M. Shia—investigation; R.L. Gallo—supervision, conceptualization, and writing (review & editing).

Disclosures: R.L. Gallo is a cofounder and consultant of MatriSys Bioscience and has equity interest in this company. No other disclosures were reported.

Submitted: 16 August 2023
Revised: 17 November 2023
Accepted: 24 January 2024

## References

Al-Sayegh, M., H. Ali, M.H. Jamal, M. ElGindi, T. Chanyong, K. Al-Awadi, and M. Abu-Farha. 2021. Mouse embryonic fibroblast adipogenic potential: A comprehensive transcriptome analysis. *Adipocyte*. 10:1–20. https://doi.org/10.1080/21623945.2020.1859789

Balabanian, K., B. Lagane, S. Infantino, K.Y. Chow, J. Harriague, B. Moepps, F. Arenzana-Seisdedos, M. Thelen, and F. Bachelerie. 2005. The chemokine SDF-1/CXCL12 binds to and signals through the orphan receptor RDC1 in T lymphocytes. *J. Biol. Chem.* 280:35760–35766. https://doi.org/10.1074/jbc.M508234200

Boehme, S.A., K. Franz-Bacon, E.P. Chen, R. Sásik, L.J. Sprague, T.W. Ly, G. Hardiman, and K.B. Bacon. 2009. A small molecule CRTH2 antagonist inhibits FITC-induced allergic cutaneous inflammation. *Int. Immunol.* 21:81–93. https://doi.org/10.1093/intimm/dxn127

Boothby, I.C., M.J. Kinet, D.P. Boda, E.Y. Kwan, S. Clancy, J.N. Cohen, I. Habrylo, M.M. Lowe, M. Pauli, A.E. Yates, et al. 2021. Early-life inflammation primes a T helper 2 cell-fibroblast niche in skin. *Nature*. 599:667–672. https://doi.org/10.1038/s41586-021-04044-7

Bouma, G., P.J. Ancliff, A.J. Thrasher, and S.O. Burns. 2010. Recent advances in the understanding of genetic defects of neutrophil number and function. *Br. J. Haematol.* 151:312–326. https://doi.org/10.1111/j.1365-2141.2010.08361.x

Brahma, P.K., H. Zhang, B.S. Murray, F.J. Shu, N. Sidell, E. Seli, and C.B. Kallen. 2012. The mRNA-binding protein Zfp36 is upregulated by β-adrenergic stimulation and represses IL-6 production in 3T3-L1 adipocytes. *Obesity*. 20:40–47. https://doi.org/10.1038/oby.2011.259

Camps, J., N. Breuls, A. Sifrim, N. Giarratana, M. Corvelyn, L. Danti, H. Grosemans, S. Vanuytven, I. Thiry, M. Belicchi, et al. 2020. Interstitial

cell remodeling promotes aberrant adipogenesis in dystrophic muscles. *Cell Rep.* 31:107597. https://doi.org/10.1016/j.celrep.2020.107597

Capucetti, A., F. Albano, and R. Bonecchi. 2020. Multiple roles for chemokines in neutrophil biology. *Front. Immunol.* 11:1259. https://doi.org/10.3389/fimmu.2020.01259

Cavagnero, K.J., and R.L. Gallo. 2022. Essential immune functions of fibroblasts in innate host defense. *Front. Immunol.* 13:1058862. https://doi.org/10.3389/fimmu.2022.1058862

Cho, J.S., E.M. Pietras, N.C. Garcia, R.I. Ramos, D.M. Farzam, H.R. Monroe, J.E. Magorien, A. Blauvelt, J.K. Kolls, A.L. Cheung, et al. 2010. IL-17 is essential for host defense against cutaneous *Staphylococcus aureus* infection in mice. *J. Clin. Invest.* 120:1762–1773. https://doi.org/10.1172/JCI40891

Cho, W.C., P. Nagarajan, Q. Ding, V.G. Prieto, and C.A. Torres-Cabala. 2022. Trichorhinophalangeal syndrome type 1-positive cells in breast dermal granulation tissues and scars: A potential diagnostic pitfall. *Am. J. Dermatopathol.* 44:964–967. https://doi.org/10.1097/DAD.0000000000002268

Chung, M.I., M. Bujnis, C.E. Barkauskas, Y. Kobayashi, and B.L.M. Hogan. 2018. Niche-mediated BMP/SMAD signaling regulates lung alveolar stem cell proliferation and differentiation. *Development*. 145:dev163014. https://doi.org/10.1242/dev.163014

Collins, C.A., and F.M. Watt. 2008. Dynamic regulation of retinoic acid-binding proteins in developing, adult and neoplastic skin reveals roles for beta-catenin and Notch signalling. *Dev. Biol.* 324:55–67. https://doi.org/10.1016/j.ydbio.2008.08.034

Davidson, S., M. Coles, T. Thomas, G. Kollias, B. Ludewig, S. Turley, M. Brenner, and C.D. Buckley. 2021. Fibroblasts as immune regulators in infection, inflammation and cancer. *Nat. Rev. Immunol.* 21:704–717. https://doi.org/10.1038/s41577-021-00540-z

Deng, C.C., Y.F. Hu, D.H. Zhu, Q. Cheng, J.J. Gu, Q.L. Feng, L.X. Zhang, Y.P. Xu, D. Wang, Z. Rong, and B. Yang. 2021. Single-cell RNA-seq reveals fibroblast heterogeneity and increased mesenchymal fibroblasts in human fibrotic skin diseases. *Nat. Commun.* 12:3709. https://doi.org/10.1038/s41467-021-24110-y

Dobin, A., C.A. Davis, F. Schlesinger, J. Drenkow, C. Zaleski, S. Jha, P. Batut, M. Chaisson, and T.R. Gingeras. 2013. STAR: Ultrafast universal RNA-seq aligner. *Bioinformatics*. 29:15–21. https://doi.org/10.1093/bioinformatics/bts635

Driskell, R.R., B.M. Lichtenberger, E. Hoste, K. Kretzschmar, B.D. Simons, M. Charalambous, S.R. Ferron, Y. Herault, G. Pavlovic, A.C. Ferguson-Smith, and F.M. Watt. 2013. Distinct fibroblast lineages determine dermal architecture in skin development and repair. *Nature*. 504:277–281. https://doi.org/10.1038/nature12783

Duffy, L., J. Henderson, M. Brown, S. Pryzborski, N. Fullard, L. Summa, J.H.W. Distler, R. Stratton, and S. O'Reilly. 2021. Bone morphogenetic protein antagonist Gremlin-1 increases myofibroblast transition in dermal fibroblasts: Implications for systemic sclerosis. *Front. Cell Dev. Biol.* 9:681061. https://doi.org/10.3389/fcell.2021.681061

Enoksson, M., C. Möller-Westerberg, G. Wicher, P.G. Fallon, K. Forsberg-Nilsson, C. Lunderius-Andersson, and G. Nilsson. 2013. Intraperitoneal influx of neutrophils in response to IL-33 is mast cell-dependent. *Blood*. 121:530–536. https://doi.org/10.1182/blood-2012-05-434209

Fajas, L., S. Miard, M.R. Briggs, and J. Auwerx. 2003. Selective cyclo-oxygenase-2 inhibitors impair adipocyte differentiation through inhibition of the clonal expansion phase. *J. Lipid Res.* 44:1652–1659. https://doi.org/10.1194/jlr.M300248-JLR200

Fossiez, F., O. Djossou, P. Chomarat, L. Flores-Romo, S. Ait-Yahia, C. Maat, J.J. Pin, P. Garrone, E. Garcia, S. Saeland, et al. 1996. T cell interleukin-17 induces stromal cells to produce proinflammatory and hematopoietic cytokines. *J. Exp. Med.* 183:2593–2603. https://doi.org/10.1084/jem.183.6.2593

Fournier, B., and D.J. Philpott. 2005. Recognition of *Staphylococcus aureus* by the innate immune system. *Clin. Microbiol. Rev.* 18:521–540. https://doi.org/10.1128/CMR.18.3.521-540.2005

Furuhashi, M., S. Saitoh, K. Shimamoto, and T. Miura. 2015. Fatty acid-binding protein 4 (FABP4): Pathophysiological insights and potent clinical biomarker of metabolic and cardiovascular diseases. *Clin. Med. Insights Cardiol.* 8:23–33. https://doi.org/10.4137/CMC.S17067

Gangwar, R.S., J.E. Gudjonsson, and N.L. Ward. 2022. Mouse models of psoriasis: A comprehensive review. *J. Invest. Dermatol.* 142:884–897. https://doi.org/10.1016/j.jid.2021.06.019

Gao, Y., X. Yao, Y. Zhai, L. Li, H. Li, X. Sun, P. Yu, T. Xue, Y. Li, and Y. Hu. 2021. Single cell transcriptional zonation of human psoriasis skin identifies an alternative immunoregulatory axis conducted by skin resident cells. *Cell Death Dis.* 12:450. https://doi.org/10.1038/s41419-021-03724-6

González-Barca, E., J. Carratalà, A. Mykietiuk, A. Fernández-Sevilla, and F. Gudiol. 2001. Predisposing factors and outcome of *Staphylococcus aureus* bacteremia in neutropenic patients with cancer. *Eur. J. Clin. Microbiol. Infect. Dis.* 20:117–119. https://doi.org/10.1007/PL00011241

Grieshaber-Bouyer, R., F.A. Radtke, P. Cunin, G. Stifano, A. Levescot, B. Vijaykumar, N. Nelson-Maney, R.B. Blaustein, P.A. Monach, P.A. Nigrovic, et al. 2021. The neutrotime transcriptional signature defines a single continuum of neutrophils across biological compartments. *Nat. Commun.* 12:2856. https://doi.org/10.1038/s41467-021-22973-9

Guo, L., X. Li, and Q.Q. Tang. 2015. Transcriptional regulation of adipocyte differentiation: A central role for CCAAT/enhancer-binding protein (C/EBP) β. *J. Biol. Chem.* 290:755–761. https://doi.org/10.1074/jbc.R114.619957

Ha, H.L., H. Wang, P. Pisitkun, J.C. Kim, I. Tassi, W. Tang, M.I. Morasso, M.C. Udey, and U. Siebenlist. 2014. IL-17 drives psoriatic inflammation via distinct, target cell-specific mechanisms. *Proc. Natl. Acad. Sci. USA*. 111:E3422–E3431. https://doi.org/10.1073/pnas.1400513111

Hall, P.R., B.O. Elmore, C.H. Spang, S.M. Alexander, B.C. Manifold-Wheeler, M.J. Castleman, S.M. Daly, M.M. Peterson, E.K. Sully, J.K. Femling, et al. 2013. Nox2 modification of LDL is essential for optimal apolipoprotein B-mediated control of agr type III *Staphylococcus aureus* quorum-sensing. *PLoS Pathog.* 9:e1003166. https://doi.org/10.1371/journal.ppat.1003166

Harshuk-Shabso, S., H. Dressler, C. Niehrs, E. Aamar, and D. Enshell-Seijffers. 2020. Fgf and Wnt signaling interaction in the mesenchymal niche regulates the murine hair cycle clock. *Nat. Commun.* 11:5114. https://doi.org/10.1038/s41467-020-18643-x

He, H., H. Suryawanshi, P. Morozov, J. Gay-Mimbrera, E. Del Duca, H.J. Kim, N. Kameyama, Y. Estrada, E. Der, J.G. Krueger, et al. 2020. Single-cell transcriptome analysis of human skin identifies novel fibroblast subpopulation and enrichment of immune subsets in atopic dermatitis. *J. Allergy Clin. Immunol.* 145:1615–1628. https://doi.org/10.1016/j.jaci.2020.01.042

Hestdal, K., F.W. Ruscetti, J.N. Ihle, S.E. Jacobsen, C.M. Dubois, W.C. Kopp, D.L. Longo, and J.R. Keller. 1991. Characterization and regulation of RB6-8C5 antigen expression on murine bone marrow cells. *J. Immunol.* 147:22–28. https://doi.org/10.4049/jimmunol.147.1.22

Hong, J.J., E.K. Hadeler, M.L. Mosca, N.D. Brownstone, T. Bhutani, and W.J. Liao. 2022. TNF-Alpha inhibitors and ustekinumab for the treatment of psoriasis: Therapeutic utility in the era of IL-17 and IL-23 inhibitors. *J. Psoriasis Psoriatic Arthritis*. 7:79–92. https://doi.org/10.1177/24755303211047479

Iwanaga, N., K. Chen, H. Yang, S. Lu, J.P. Hoffmann, A. Wanek, J.E. McCombs, K. Song, J. Rangel-Moreno, E.B. Norton, and J.K. Kolls. 2021. Vaccine-driven lung TRM cells provide immunity against Klebsiella via fibroblast IL-17R signaling. *Sci. Immunol.* 6:eabf1198. https://doi.org/10.1126/sciimmunol.abf1198

Janson, D.G., G. Saintigny, A. van Adrichem, C. Mahé, and A. El Ghalbzouri. 2012. Different gene expression patterns in human papillary and reticular fibroblasts. *J. Invest. Dermatol.* 132:2565–2572. https://doi.org/10.1038/jid.2012.192

Jin, S., C.F. Guerrero-Juarez, L. Zhang, I. Chang, R. Ramos, C.H. Kuan, P. Myung, M.V. Plikus, and Q. Nie. 2021. Inference and analysis of cell-cell communication using CellChat. *Nat. Commun.* 12:1088. https://doi.org/10.1038/s41467-021-21246-9

Joost, S., K. Annusver, T. Jacob, X. Sun, T. Dalessandri, U. Sivan, I. Sequeira, R. Sandberg, and M. Kasper. 2020. The molecular anatomy of mouse skin during hair growth and rest. *Cell Stem Cell*. 26:441–457.e7. https://doi.org/10.1016/j.stem.2020.01.012

Karlsen, J.R., N. Borregaard, and J.B. Cowland. 2010. Induction of neutrophil gelatinase-associated lipocalin expression by co-stimulation with interleukin-17 and tumor necrosis factor-alpha is controlled by IkappaB-zeta but neither by C/EBP-beta nor C/EBP-delta. *J. Biol. Chem.* 285:14088–14100. https://doi.org/10.1074/jbc.M109.017129

Kimball, A.B., G.B.E. Jemec, A. Alavi, Z. Reguiai, A.B. Gottlieb, F.G. Bechara, C. Paul, E.J. Giamarellos Bourboulis, A.P. Villani, A. Schwinn, et al. 2023. Secukinumab in moderate-to-severe hidradenitis suppurativa (SUNSHINE and SUNRISE): Week 16 and week 52 results of two identical, multicentre, randomised, placebo-controlled, double-blind phase 3 trials. *Lancet*. 401:747–761. https://doi.org/10.1016/S0140-6736(23)00022-3

Kramann, R., S.V. Fleig, R.K. Schneider, S.L. Fabian, D.P. DiRocco, O. Maarouf, J. Wongboonsin, Y. Ikeda, D. Heckl, S.L. Chang, et al. 2015. Pharmacological GLI2 inhibition prevents myofibroblast cell-cycle progression and reduces kidney fibrosis. *J. Clin. Invest.* 125:2935–2951. https://doi.org/10.1172/JCI74929

Kwack, M.H., M.K. Kim, J.C. Kim, and Y.K. Sung. 2013. Wnt5a attenuates Wnt/β-catenin signalling in human dermal papilla cells. *Exp. Dermatol.* 22:229–231. https://doi.org/10.1111/exd.12101

Lasrich, D., A. Bartelt, T. Grewal, and J. Heeren. 2015. Apolipoprotein E promotes lipid accumulation and differentiation in human adipocytes. *Exp. Cell Res.* 337:94–102. https://doi.org/10.1016/j.yexcr.2015.07.015

Lehman, H.K., and B.H. Segal. 2020. The role of neutrophils in host defense and disease. *J. Allergy Clin. Immunol.* 145:1535–1544. https://doi.org/10.1016/j.jaci.2020.02.038

Li, K., J. Zhao, M. Wang, L. Niu, Y. Wang, Y. Li, and Y. Zheng. 2021. The roles of various prostaglandins in fibrosis: A review. *Biomolecules*. 11:11. https://doi.org/10.3390/biom11060789

Li, X., R. Bechara, J. Zhao, M.J. McGeachy, and S.L. Gaffen. 2019. IL-17 receptor-based signaling and implications for disease. *Nat. Immunol.* 20:1594–1602. https://doi.org/10.1038/s41590-019-0514-y

Liao, Y., G.K. Smyth, and W. Shi. 2019. The R package Rsubread is easier, faster, cheaper and better for alignment and quantification of RNA sequencing reads. *Nucleic Acids Res.* 47:e47. https://doi.org/10.1093/nar/gkz114

Liu, J., H.W. Chang, R. Grewal, D.D. Cummins, A. Bui, K.M. Beck, S. Sekhon, D. Yan, Z.M. Huang, T.H. Schmidt, et al. 2021. Transcriptomic profiling of plaque psoriasis and cutaneous T-cell subsets during treatment with secukinumab. *JID Innov.* 2:100094. https://doi.org/10.1016/j.xjidi.2021.100094

Love, M.I., W. Huber, and S. Anders. 2014. Moderated estimation of fold change and dispersion for RNA-seq data with DESeq2. *Genome Biol.* 15:550. https://doi.org/10.1186/s13059-014-0550-8

Ma, F., O. Plazyo, A.C. Billi, L.C. Tsoi, X. Xing, R. Wasikowski, M. Gharaee-Kermani, G. Hile, Y. Jiang, P.W. Harms, et al. 2023. Single cell and spatial sequencing define processes by which keratinocytes and fibroblasts amplify inflammatory responses in psoriasis. *Nat. Commun.* 14:3455. https://doi.org/10.1038/s41467-023-39020-4

Marangoni, R.G., P. Datta, A. Paine, S. Duemmel, M. Nuzzo, L. Sherwood, J. Varga, C. Ritchlin, and B.D. Korman. 2022. Thy-1 plays a pathogenic role and is a potential biomarker for skin fibrosis in scleroderma. *JCI Insight*. 7:e149426. https://doi.org/10.1172/jci.insight.149426

Marcelin, G., A. Ferreira, Y. Liu, M. Atlan, J. Aron-Wisnewsky, V. Pelloux, Y. Botbol, M. Ambrosini, M. Fradet, C. Rouault, et al. 2017. A PDGFRα-mediated switch toward $CD9^{high}$ adipocyte progenitors controls obesity-induced adipose tissue fibrosis. *Cell Metab.* 25:673–685. https://doi.org/10.1016/j.cmet.2017.01.010

Mathew, S.J., J.M. Hansen, A.J. Merrell, M.M. Murphy, J.A. Lawson, D.A. Hutcheson, M.S. Hansen, M. Angus-Hill, and G. Kardon. 2011. Connective tissue fibroblasts and Tcf4 regulate myogenesis. *Development*. 138:371–384. https://doi.org/10.1242/dev.057463

McGeachy, M.J., D.J. Cua, and S.L. Gaffen. 2019. The IL-17 family of cytokines in health and disease. *Immunity*. 50:892–906. https://doi.org/10.1016/j.immuni.2019.03.021

McGinnis, C.S., L.M. Murrow, and Z.J. Gartner. 2019. DoubletFinder: Doublet detection in single-cell RNA sequencing data using artificial nearest neighbors. *Cell Syst.* 8:329–337.e4. https://doi.org/10.1016/j.cels.2019.03.003

Mehta, H.M., and S.J. Corey. 2021. G-CSF, the guardian of granulopoiesis. *Semin. Immunol.* 54:101515. https://doi.org/10.1016/j.smim.2021.101515

Merrick, D., A. Sakers, Z. Irgebay, C. Okada, C. Calvert, M.P. Morley, I. Percec, and P. Seale. 2019. Identification of a mesenchymal progenitor cell hierarchy in adipose tissue. *Science*. 364:eaav2501. https://doi.org/10.1126/science.aav2501

Metzemaekers, M., M. Gouwy, and P. Proost. 2020. Neutrophil chemoattractant receptors in health and disease: Double-edged swords. *Cell. Mol. Immunol.* 17:433–450. https://doi.org/10.1038/s41423-020-0412-0

Miller, L.S., and J.S. Cho. 2011. Immunity against *Staphylococcus aureus* cutaneous infections. *Nat. Rev. Immunol.* 11:505–518. https://doi.org/10.1038/nri3010

Mölne, L., M. Verdrengh, and A. Tarkowski. 2000. Role of neutrophil leukocytes in cutaneous infection caused by *Staphylococcus aureus*. *Infect. Immun.* 68:6162–6167. https://doi.org/10.1128/IAI.68.11.6162-6167.2000

Moos, S., A.N. Mohebiany, A. Waisman, and F.C. Kurschus. 2019. Imiquimod-induced psoriasis in mice depends on the IL-17 signaling of keratinocytes. *J. Invest. Dermatol.* 139:1110–1117. https://doi.org/10.1016/j.jid.2019.01.006

Moos, S., Regen, T., Wanke, F., Tian, Y., Arendholz, L.T., Hauptmann, J., Heinen, A.P., Bleul, L., Bier, K., El Malki, K., et al. 2023. IL-17 Signaling in keratinocytes orchestrates the defense against *Staphylococcus aureus* skin infection. *J Invest Dermatol.* 143:1257–1267.e10. https://doi.org/10.1016/j.jid.2023.01.016

Nakatsuji, T., S.L. Brinton, K.J. Cavagnero, A.M. O'Neill, Y. Chen, T. Dokoshi, A.M. Butcher, O.C. Osuoji, F. Shafiq, J.L. Espinoza, et al. 2023. Competition between skin antimicrobial peptides and commensal bacteria in type 2 inflammation enables survival of *S. aureus*. *Cell Rep.* 42:112494. https://doi.org/10.1016/j.celrep.2023.112494

Nallanthighal, S., J.P. Heiserman, and D.J. Cheon. 2021. Collagen type XI alpha 1 (COL11A1): A novel biomarker and a key player in cancer. *Cancers*. 13:935. https://doi.org/10.3390/cancers13050935

Nizet, V., T. Ohtake, X. Lauth, J. Trowbridge, J. Rudisill, R.A. Dorschner, V. Pestonjamasp, J. Piraino, K. Huttner, and R.L. Gallo. 2001. Innate antimicrobial peptide protects the skin from invasive bacterial infection. *Nature*. 414:454–457. https://doi.org/10.1038/35106587

Phan, Q.M., G.M. Fine, L. Salz, G.G. Herrera, B. Wildman, I.M. Driskell, and R.R. Driskell. 2020. Lef1 expression in fibroblasts maintains developmental potential in adult skin to regenerate wounds. *Elife*. 9:e60066. https://doi.org/10.7554/eLife.60066

Philippeos, C., S.B. Telerman, B. Oulès, A.O. Pisco, T.J. Shaw, R. Elgueta, G. Lombardi, R.R. Driskell, M. Soldin, M.D. Lynch, and F.M. Watt. 2018. Spatial and single-cell transcriptional profiling identifies functionally distinct human dermal fibroblast subpopulations. *J. Invest. Dermatol.* 138:811–825. https://doi.org/10.1016/j.jid.2018.01.016

Rockey, D.C., N. Weymouth, and Z. Shi. 2013. Smooth muscle α actin (Acta2) and myofibroblast function during hepatic wound healing. *PLoS One*. 8:e77166. https://doi.org/10.1371/journal.pone.0077166

Rodríguez-Cerdeira, C., J.L. González-Cespón, E. Martínez-Herrera, M. Carnero-Gregorio, A. López-Barcenas, A. Sergeev, and D.M. Saunte. 2021. Candida infections in patients with psoriasis and psoriatic arthritis treated with interleukin-17 inhibitors and their practical management. *Ital. J. Dermatol. Venereol.* 156:545–557. https://doi.org/10.23736/S2784-8671.20.06580-3

Rognoni, E., C. Gomez, A.O. Pisco, E.L. Rawlins, B.D. Simons, F.M. Watt, and R.R. Driskell. 2016. Inhibition of β-catenin signalling in dermal fibroblasts enhances hair follicle regeneration during wound healing. *Development*. 143:2522–2535. https://doi.org/10.1242/dev.131797

Rose-John, S., K. Winthrop, and L. Calabrese. 2017. The role of IL-6 in host defence against infections: Immunobiology and clinical implications. *Nat. Rev. Rheumatol.* 13:399–409. https://doi.org/10.1038/nrrheum.2017.83

Schauber, J., and R.L. Gallo. 2009. Antimicrobial peptides and the skin immune defense system. *J. Allergy Clin. Immunol.* 124:R13–R18. https://doi.org/10.1016/j.jaci.2009.07.014

Schmid, A., T. Karrasch, and A. Schäffler. 2021. Meteorin-like protein (Metrnl) in obesity, during weight loss and in adipocyte differentiation. *J. Clin. Med.* 10:4338. https://doi.org/10.3390/jcm10194338

Shao, S., T. Cao, L. Jin, B. Li, H. Fang, J. Zhang, Y. Zhang, J. Hu, and G. Wang. 2016. Increased lipocalin-2 contributes to the pathogenesis of psoriasis by modulating neutrophil chemotaxis and cytokine secretion. *J. Invest. Dermatol.* 136:1418–1428. https://doi.org/10.1016/j.jid.2016.03.002

Shin, M.K., B. Choi, E.Y. Kim, J.E. Park, E.S. Hwang, H.J. Lee, M.K. Kim, J.E. Kim, S.W. Kim, and E.J. Chang. 2018. Elevated Pentraxin 3 in obese adipose tissue promotes adipogenic differentiation by activating neuropeptide Y signaling. *Front. Immunol.* 9:1790. https://doi.org/10.3389/fimmu.2018.01790

Singh, S., Y.S. Rajput, A.K. Barui, R. Sharma, and S. Grover. 2015. Expression of developmental genes in brown fat cells grown in vitro is linked with lipid accumulation. *In Vitro Cell. Dev. Biol. Anim.* 51:1003–1011. https://doi.org/10.1007/s11626-015-9930-y

Slowikowski, K., H.N. Nguyen, E.H. Noss, D.P. Simmons, F. Mizoguchi, G.F.M. Watts, M.F. Gurish, M.B. Brenner, and S. Raychaudhuri. 2020. CUX1 and IκBζ (NFKBIZ) mediate the synergistic inflammatory response to TNF and IL-17A in stromal fibroblasts. *Proc. Natl. Acad. Sci. USA*. 117:5532–5541. https://doi.org/10.1073/pnas.1912702117

Solé-Boldo, L., G. Raddatz, S. Schütz, J.P. Mallm, K. Rippe, A.S. Lonsdorf, M. Rodríguez-Paredes, and F. Lyko. 2020. Single-cell transcriptomes of the human skin reveal age-related loss of fibroblast priming. *Commun. Biol.* 3:188. https://doi.org/10.1038/s42003-020-0922-4

Stark, K., A. Eckart, S. Haidari, A. Tirniceriu, M. Lorenz, M.L. von Brühl, F. Gärtner, A.G. Khandoga, K.R. Legate, R. Pless, et al. 2013. Capillary and arteriolar pericytes attract innate leukocytes exiting through venules and "instruct" them with pattern-recognition and motility programs. *Nat. Immunol.* 14:41–51. https://doi.org/10.1038/ni.2477

Wang, S.M., R.D. Hwang, A.S. Greenberg, and H.L. Yeo. 2003. Temporal and spatial assembly of lipid droplet-associated proteins in 3T3-L1 preadipocytes. *Histochem. Cell Biol.* 120:285–292. https://doi.org/10.1007/s00418-003-0575-7

Xu, Z., D. Chen, Y. Hu, K. Jiang, H. Huang, Y. Du, W. Wu, J. Wang, J. Sui, W. Wang, et al. 2021. Anatomically distinct fibroblast subsets determine skin autoimmune patterns. *Nature*. 601:118–124. https://doi.org/10.1038/s41586-021-04221-8

Young, M.D., and S. Behjati. 2020. SoupX removes ambient RNA contamination from droplet-based single-cell RNA sequencing data. *Gigascience*. 9:giaa151. https://doi.org/10.1093/gigascience/giaa151

Yu, G., L.G. Wang, Y. Han, and Q.Y. He. 2012. clusterProfiler: An R package for comparing biological themes among gene clusters. *OMICS*. 16: 284–287. https://doi.org/10.1089/omi.2011.0118

Zachara, M., P.Y. Rainer, H. Hashimi, J.M. Russeil, D. Alpern, R. Ferrero, M. Litovchenko, and B. Deplancke. 2022. Mammalian adipogenesis regulator (Areg) cells use retinoic acid signalling to be non- and anti-adipogenic in age-dependent manner. *EMBO J.* 41:e108206. https://doi.org/10.15252/embj.2021108206

Zhang, B., P.C. Tsai, M. Gonzalez-Celeiro, O. Chung, B. Boumard, C.N. Perdigoto, E. Ezhkova, and Y.C. Hsu. 2016. Hair follicles' transit-amplifying cells govern concurrent dermal adipocyte production through Sonic Hedgehog. *Genes Dev.* 30:2325–2338. https://doi.org/10.1101/gad.285429.116

Zhang, L.J., S.X. Chen, C.F. Guerrero-Juarez, F. Li, Y. Tong, Y. Liang, M. Liggins, X. Chen, H. Chen, M. Li, et al. 2019. Age-related loss of innate immune antimicrobial function of dermal fat is mediated by transforming growth factor beta. *Immunity*. 50:121–136.e5. https://doi.org/10.1016/j.immuni.2018.11.003

Zhang, L.J., C.F. Guerrero-Juarez, T. Hata, S.P. Bapat, R. Ramos, M.V. Plikus, and R.L. Gallo. 2015. Innate immunity. Dermal adipocytes protect against invasive *Staphylococcus aureus* skin infection. *Science*. 347:67–71. https://doi.org/10.1126/science.1260972

Zheng, Z., Y.N. Li, S. Jia, M. Zhu, L. Cao, M. Tao, J. Jiang, S. Zhan, Y. Chen, P.J. Gao, et al. 2021. Lung mesenchymal stromal cells influenced by Th2 cytokines mobilize neutrophils and facilitate metastasis by producing complement C3. *Nat. Commun.* 12:6202. https://doi.org/10.1038/s41467-021-26460-z

# Supplemental material

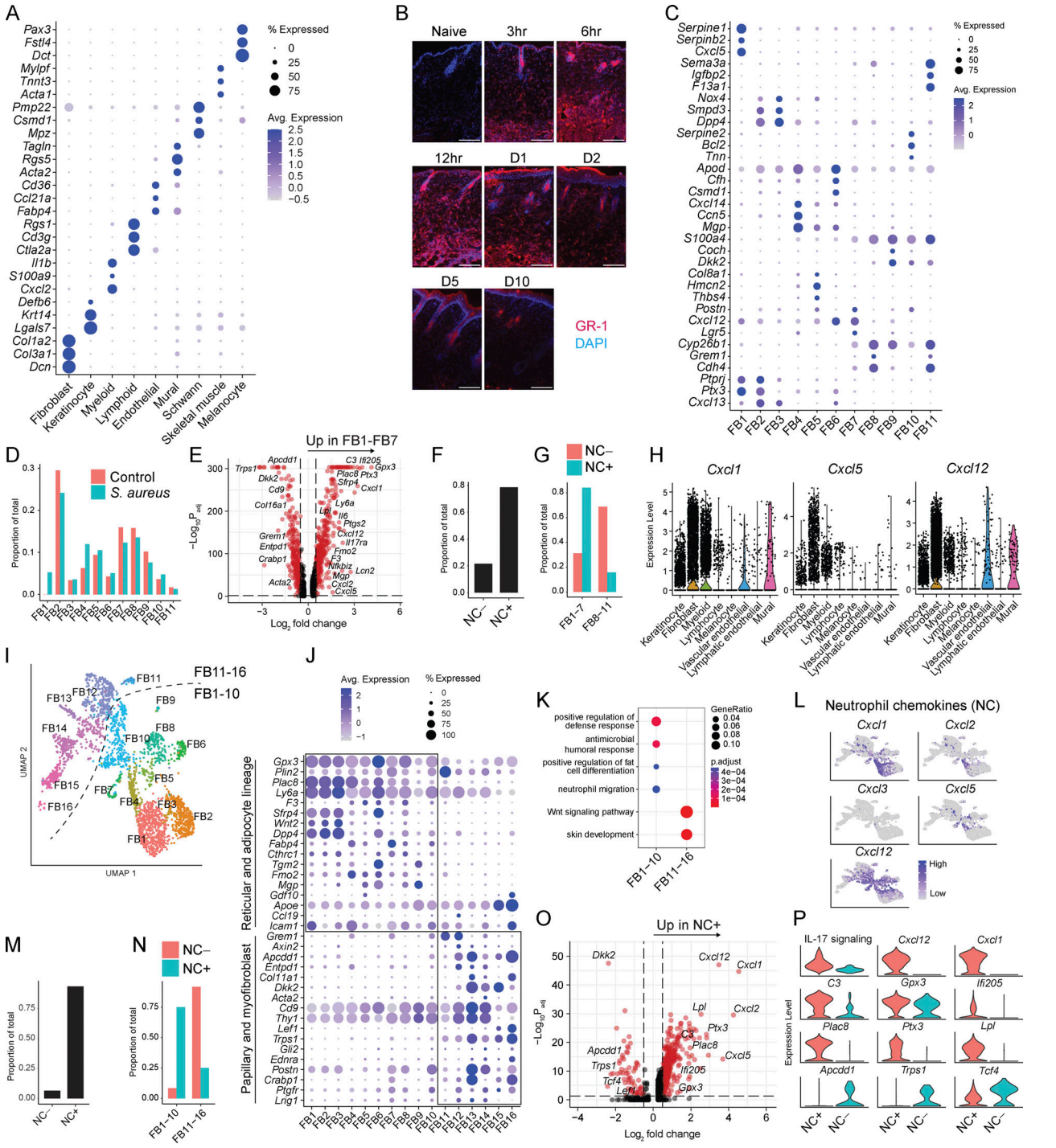


Figure S1. **CXCL12+ dermal fibroblast–neutrophil communication during *S. aureus* infection. (A–E)** Mouse back skin with intradermal *S. aureus* infection. **(A and C–E)** scRNA-Seq with data obtained from samples pooled from the skin of $N = 4$ mice independently treated in each group. **(A)** Expression of top three cell type marker genes. **(B)** Representative GR-1 (neutrophils) immunostaining. Scale bar, 150 µm. **(C)** Expression of top three fibroblast cluster marker genes. **(D)** Frequency of fibroblast clusters in infected and control mice. **(E)** DEGs between FB1–FB7 and FB8–FB11 during infection using Wilcoxon Rank Sum test. $Log_2$ fold-change and P value (adjusted) cut-offs are 0.5 and 0.05, respectively. **(F)** Frequency of neutrophil chemokine+/− fibroblast during infection. **(G)** Frequency of neutrophil chemokine+/− cells across FB1–FB7 and FB8–FB11 during infection. **(H–P)** Analysis of scRNA-Seq data from mouse back skin with *S. aureus* epicutaneous infection. Samples were pooled from the skin of $N = 5$ mice independently treated in each group. **(H)** Expression of neutrophil chemokines across cell types. **(I)** Fibroblast dimensionality reduction colored by cluster. Dashed line separates FB1–FB10 and FB11–FB16. **(J)** Expression of fibroblast subset markers across clusters. Boxes highlight high expression of reticular and adipocyte lineage genes in FB1–FB10 and high expression of papillary and myofibroblast genes in FB11–FB16. **(K)** GO term analysis comparing FB1–FB10 and FB11–FB16. **(L)** Neutrophil chemokine expression across fibroblast clusters. **(M)** Frequency of neutrophil chemokine+/− fibroblast during infection. **(N)** Frequency of neutrophil chemokine+/− cells across FB1–10 and FB11–16 during infection. **(O)** DEGs between neutrophil chemokine+ and neutrophil chemokine− fibroblasts during infection using Wilcoxon Rank Sum test. $Log_2$ fold-change and P value (adjusted) cut-offs are 0.5 and 0.05, respectively. **(P)** Expression of neutrophil chemokine+/− fibroblast markers during infection.

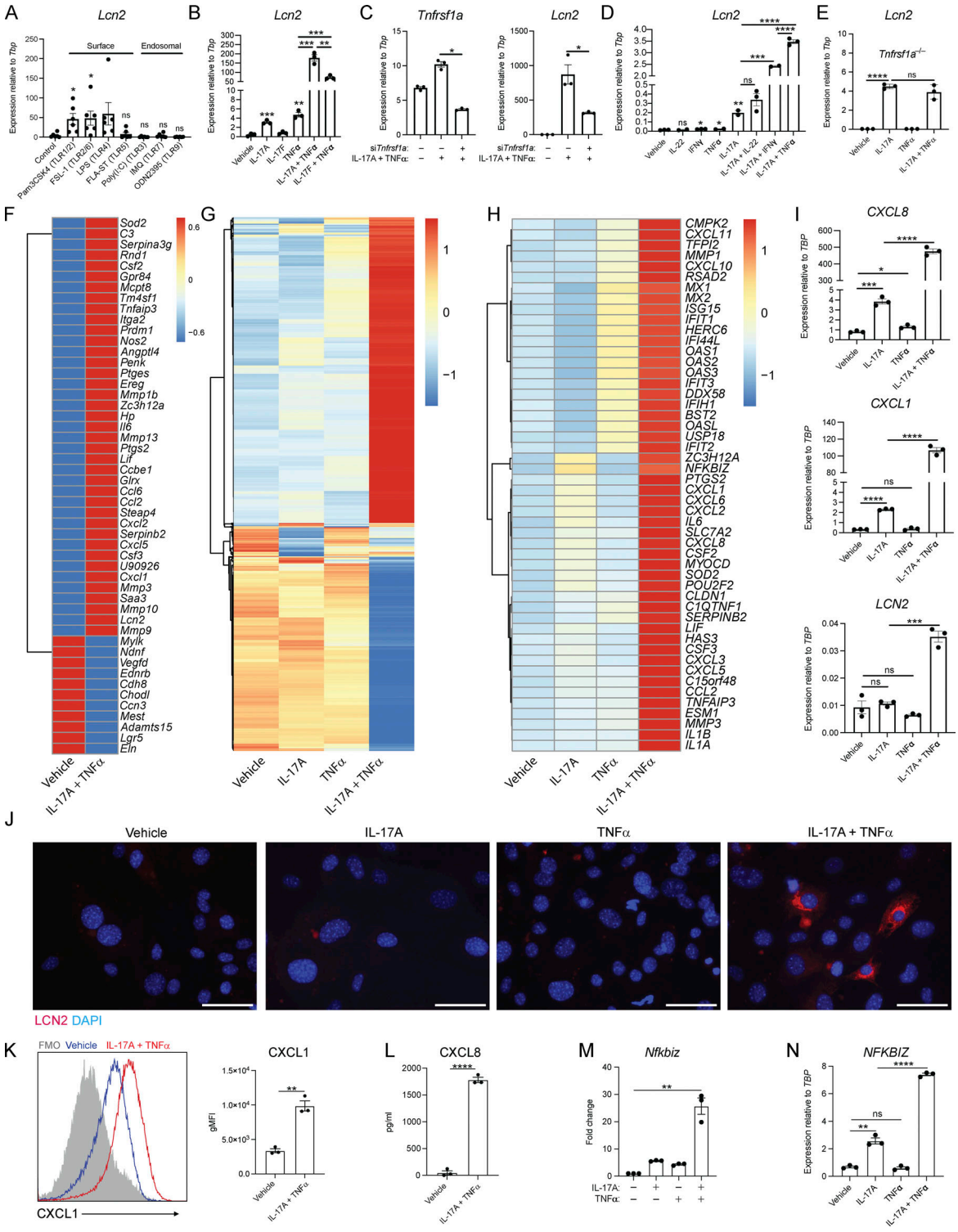

Figure S2. **IL-17 and TNFα activate preadipocyte fibroblasts. (A and B)** Gene expression in 3T3-L1 fibroblasts by qPCR following stimulation with (A) toll ligands (data pooled from two independent experiments with *N* = 3) and (B) recombinant cytokines. **(C)** Gene expression in 3T3-L1s by qPCR following *Tnfrsrf1a* or scramble control siRNA knockdown and subsequent stimulation with recombinant cytokines. **(D and E)** Gene expression in WT (D) and *Tnfrsrf1a*$^{-/-}$ (E) primary MDFBs by qPCR following stimulation with recombinant cytokines. **(F)** Expression of top 50 variable genes per group in MDFBs by bulk RNA-Seq, scaled by row. Data were obtained from samples pooled from *N* = 3 independent biological replicates in each group. **(G and H)** HPADs stimulated with recombinant cytokines. Expression of top 2,000 (G) and top 50 (H) variable genes by bulk RNA-Seq, scaled by row. Data were obtained from samples pooled from *N* = 3 independent biological replicates in each group. **(I)** Gene expression by qPCR. **(J)** Representative LCN2 immunostaining in MDFB. Scale bar, 150 µm. **(K)** Representative CXCL1 intracellular cytokine staining (left) and quantification (right) in primary MDFBs. **(L)** CXCL8 ELISA with HPAD CM. **(M and N)** MDFB (M) and HPAD (N) gene expression by qPCR following addition of recombinant cytokines. Data in B–N are representative of at least two independent experiments with *N* = 2–3. FMO, fluorescence minus one; ns (not significant), *P < 0.05, **P < 0.01, ***P < 0.001, and ****P < 0.0001 using unpaired *t* test.

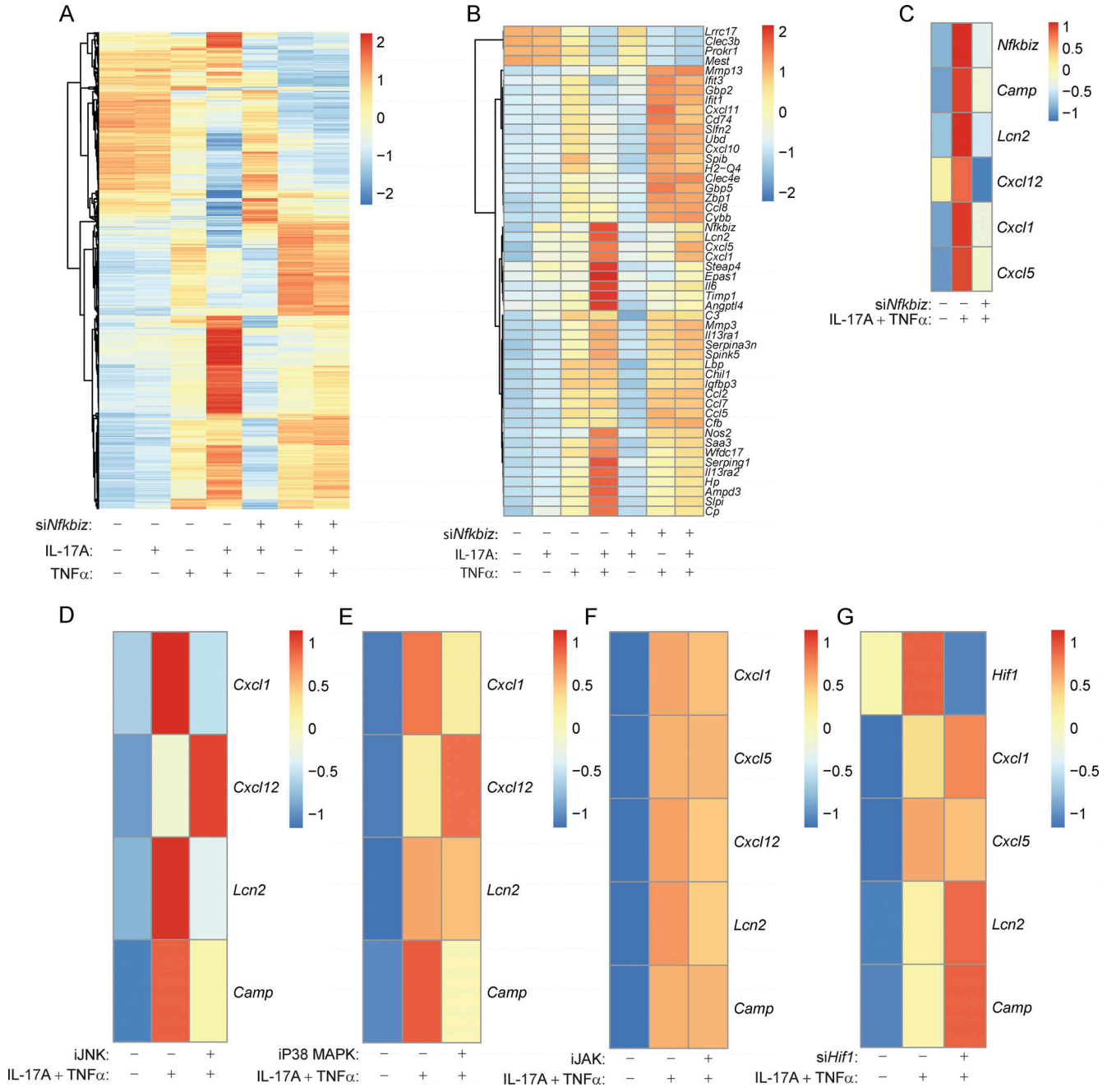


Figure S3. **Mechanism of preadipocyte fibroblast activation by IL-17A and TNFα. (A and B)** Expression of top 2,000 (A) and top 50 (B) variable genes in 3T3-L1 fibroblasts by bulk RNA-Seq following *Nfkbiz* siRNA knockdown and subsequent stimulation with recombinant cytokines. Data were obtained from samples pooled from *N* = 3 independent biological replicates in each group. **(C)** DEGs in 3T3-L1s by qPCR following *Nfkbiz* siRNA knockdown. Averages shown for *N* = 3. **(D–F)** Gene expression in 3T3-L1s by qPCR following pharmacological inhibition of JNK (D), P38 MAPK (E), and JAK (F). Averages shown for *N* = 3. **(G)** Gene expression in 3T3-L1s by qPCR following *Hif1* siRNA knockdown or scramble control siRNA knockdown. Averages shown for *N* = 3. Heatmaps were all scaled by row. Data in A–G are representative of at least two independent experiments.

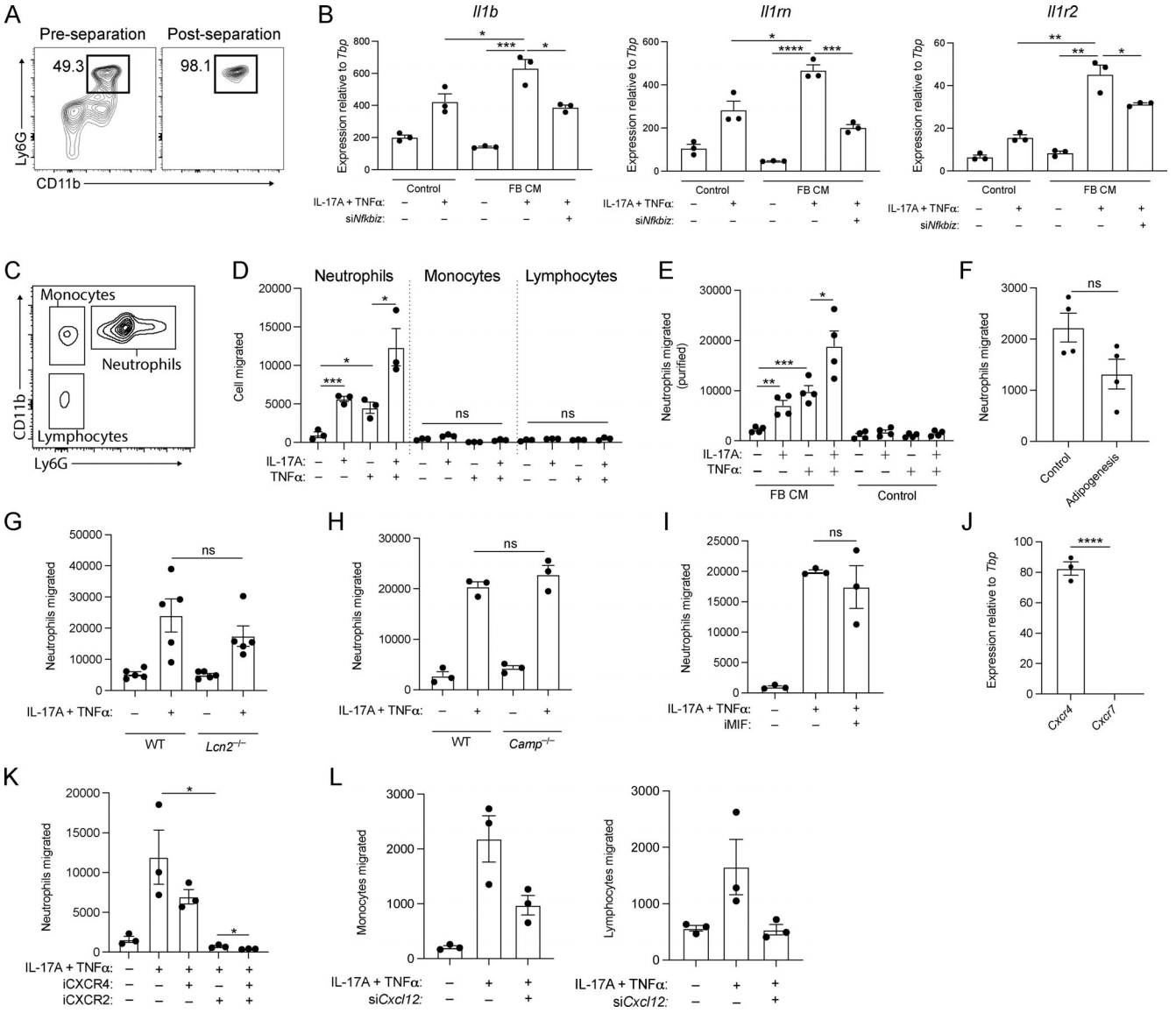


Figure S4. **CXCL12+ fibroblast–neutrophil communication in vitro. (A)** Representative bone marrow neutrophil (CD11b+Ly6G+) purity following magnetic bead separation. **(B)** qPCR of neutrophil activation markers following stimulation with 3T3-L1 fibroblast CM. Fibroblasts were treated with *Nfkbiz* siRNA or scramble control then IL-17A and TNFα. **(C)** Flow cytometry gating strategy. **(D)** Leukocyte migration assay with primary MDFB CM. **(E and F)** Migration assay with purified neutrophils using CM from 3T3-L1 fibroblast treated IL-17A and TNFα (E) or adipocyte differentiation media (adipogenesis) (F). **(G)** Migration assay with WT and *Lcn2*$^{-/-}$ MDFB CM. Data were pooled from two independent experiments with $N = 2–3$. **(H)** Migration assay with WT and *Camp*$^{-/-}$ MDFB CM. **(I)** Migration assay using 3T3-L1 fibroblast CM pretreated with MIF pharmacological inhibitor. **(J)** Expression of CXCL12 receptors in purified bone marrow neutrophils by qPCR. **(K)** Migration assay with MDFB CM and pharmacological inhibitors targeting CXCR2 and CXCR4. **(L)** Migration assay using CM from 3T3-L1s with *Cxcl12* or scramble control siRNA knockdown. Data in A–B, D–F, and H–L are representative of two to three independent experiments with $N = 3$. ns (not significant), *P < 0.05, **P < 0.01, ***P < 0.001, and ****P < 0.0001 using unpaired *t* test.

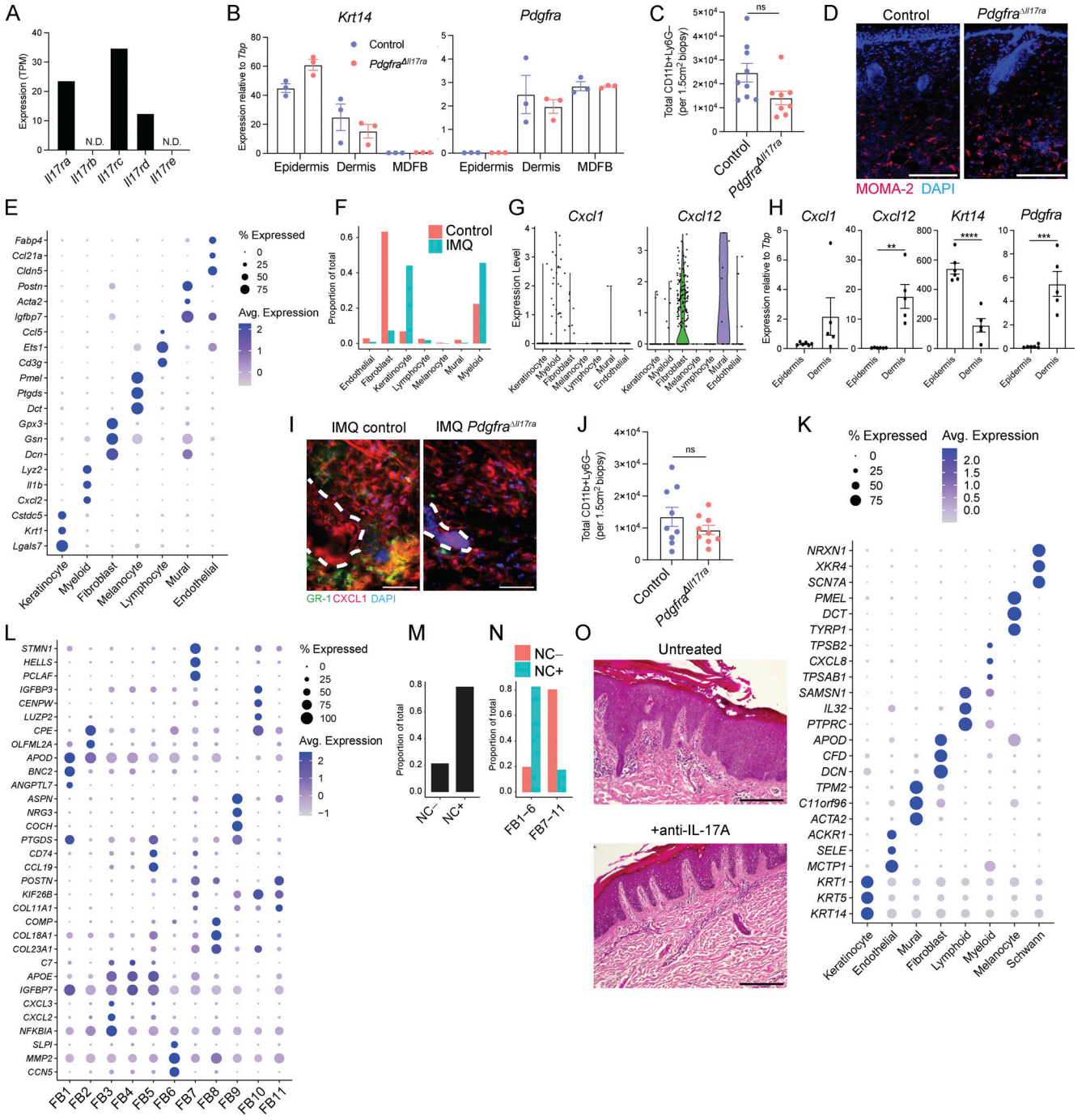


Figure S5. **Dermal fibroblast recognition of IL-17 in murine and human type 17 inflammation. (A)** Gene expression by bulk RNA-Seq in primary MDFBs from Fig. S2. Data were obtained from samples pooled from three independent biological replicates in each group. **(B)** *Krt14* and *Pdgfra* expressions were measured by qPCR in separated epidermis, dermis, and isolated MDFB from the skin of *Pdgfra*$^{\Delta Il17ra}$ and Cre− control mice. Data are representative of two independent experiments with *N* = 3 mice. **(C)** Total live CD11b+Ly6G−CD45$^+$ cells (monocytes and macrophages) in rmIL-17A and rmTNFα challenged mouse skin on day 3. Data were pooled from three independent experiments with *N* = 2–3 mice. **(D)** Representative MOMA-2 (monocytes and macrophages) immunostaining on day 2 after i.d. *S. aureus* infection. Scale bar, 150 µm. **(E–J)** Mouse back skin in IMQ model. **(E–G)** scRNA-Seq analysis. Data were obtained from samples pooled from skin of *N* = 4 mice independently treated in each group. **(E)** Expression of top 3 marker genes for each cell type. **(F)** Proportion of each cell type in mice treated with IMQ or vehicle (control). **(G)** Gene expression across cell types. **(H)** Gene expression by qPCR in enzymatically separated epidermis and dermis following IMQ treatment. Data are representative of two independent experiments with *N* = 3 mice. **(I)** Representative GR-1 (neutrophils) and CXCL1 immunostaining. Scale bar, 50 µm. Dashed lines outline hair follicles. **(J)** Total live CD11b+Ly6G−CD45$^+$ cells (monocytes and macrophages) in IMQ-treated mice. Data were pooled from three independent experiments with *N* = 3 mice. **(K–M)** Human psoriasis (*N* = 3 donors) and healthy control (*N* = 3 donors) skin scRNA-Seq. **(K)** Expression of top three marker genes for each cell type. **(L)** Expression of top three marker genes for each fibroblast cluster. **(M)** Frequency of neutrophil chemokine+/− fibroblast in psoriasis. **(N)** Frequency of neutrophil chemokine+/− cells across FB1–FB6 and FB7–FB11 in psoriasis. **(O)** Representative H&E staining of lesional skin biopsies with and without anti–IL-17 treatment. Scale bar, 300 µm. N.D. (not detected), ns (not significant), **P < 0.01, ***P < 0.001, and ****P < 0.0001 using unpaired *t* test.

**Provided online are Table S1 and Table S2. Table S1 shows fibroblast subset markers. Table S2 shows RT-qPCR primers.**